DENND5A-related developmental and epileptic encephalopathy driven by loss of symmetric cell division of apical neural progenitors

Emily Banks[1], Vincent Francis[1], Sheng-Jia Lin[2], Fares Kharfallah[1], Vladimir Fonov[1], Maxime Levesque[1], Chanshuai Han[1], Gopinath Kulasekaran[1], Marius Tuznik[1], Armin Bayati[1], Reem Al-Khater[3], Fowzan S. Alkuraya[4], Loukas Argyriou[5], Meisam Babaei[6], Melanie Bahlo[7], Behnoosh Bakhshoodeh[8], Eileen Barr[9], Lauren Bartik[10,11], Mahmoud Bassiony[12], Miriam Bertrand[13], Dominique Braun[14], Rebecca Buchert[13], Mauro Budetta[15], Maxime Cadieux-Dion[16], Daniel Calame[17-19], Heidi Cope[20], Donna Cushing[21], Stephanie Efthymiou[22], Marwa A. Elmaksoud[23], Huda G. El Said[24], Tawfiq Froukh[25], Harinder K. Gill[26], Joseph G. Gleeson[27,28], Laura Gogoll[14], Elaine S.-Y. Goh[21], Vykuntaraju K Gowda[29], Tobias B. Haack[13], Mais O. Hashem[4], Stefan Hauser[30,31], Trevor L. Hoffman[32], Jacob S. Hogue[33], Akimoto Hosokawa[34], Henry Houlden[22], Kevin Huang[2], Stephanie Huynh[26], Ehsan G. Karimiani[35,36], Silke Kaulfuß[5], G. Christoph Korenke[37], Amy Kritzer[38], Hane Lee[39], James R. Lupski[17-19,40], Elysa J. Marco[41], Kirsty McWalter[42], Arakel Minassian[43], Berge A. Minassian[44], David Murphy[22], Juanita Neira-Fresneda[9], Hope Northrup[45], Denis Nyaga[34], Barbara Oehl-Jaschkowitz[46], Matthew Osmond[47], Richard Person[42], Davut Pehlivan[17-19], Cassidy Petree[2], Lynette G. Sadleir[34], Carol Saunders[10,16,48], Ludger Schoels[30,31], Vandana Shashi[20], Rebecca C. Spillman[20], Varunvenkat M. Srinivasan[29], Tulay Tos[49], Undiagnosed Diseases Network[†], Maha S. Zaki[50], Dihong Zhou[10,11], Christiane Zweier[14], Jean-François Trempe[51], Thomas M. Durcan[1], Ziv Gan-Or[1,52], Massimo Avoli[1], Cesar Alves[53], Guarav K. Varshney[2], Reza Maroofian[22], David A. Rudko[1], Peter S. McPherson[1].

[1] Department of Neurology and Neurosurgery, Montreal Neurological Institute, McGill University, Montréal, QC H3A 2B4, Canada

[2] Genes & Human Disease Research Program, Oklahoma Medical Research Foundation, Oklahoma City, OK, 73104, USA

[3] Johns Hopkins Aramco Healthcare, Dhahran 34465, Saudi Arabia

[4] Department of Translational Genomics, Center for Genomic Medicine, King Faisal Specialist Hospital and Research Center, Riyadh 11211, Saudi Arabia

[5] Institute of Human Genetics, University Medical Center, Göttingen 37073, Germany

[6] Department of Pediatrics, North Khorasan University of Medical Sciences, Bojnurd, Iran

[7] Walter and Eliza Hall Institute for Medical Research, Parkville Victoria 3052, Australia

[8] Mashhad University of Medical Sciences, Mashhad, Iran

[9] Emory University, Department of Human Genetics, Atlanta, GA 30322, USA

[10] University of Missouri-Kansas City, School of Medicine, Kansas City, MO 64108, USA

[11] Department of Pediatrics, Division of Clinical Genetics, Children's Mercy Hospital, Kansas City, MO 64108, USA

[12] Faculty of Medicine, Alexandria University, Alexandria, Egypt

[13] Institute of Medical Genetics and Applied Genomics, University of Tübingen, Tübingen 72076, Germany

[14] Department of Human Genetics, Inselspital, Bern University Hospital, University of Bern, Bern, Switzerland

[15] Paediatric and Child Neurology Unit, Cava de' Tirreni AOU S. Giovanni di Dio e Ruggiero d'Aragona Hospital, Salerno, Italy

[16] Department of Pathology and Laboratory Medicine, Children's Mercy Hospital, Kansas City, MO 64108, USA

[17] Department of Pediatrics, Baylor College of Medicine, Houston, TX, USA

[18] Texas Children's Hospital, Houston, TX, USA

[19] Department of Molecular and Human Genetics, Baylor College of Medicine, Houston, TX, USA

[20] Division of Medical Genetics, Department of Pediatrics, Duke University Medical Center, Durham, NC 27710, USA

[21] Laboratory Medicine and Genetics, Trillium Health Partners, Mississauga, ON L5B 1B8, Canada

[22] Department of Neuromuscular Diseases, University College London (UCL) Institute of Neurology, Queen Square, London, WC1N 3BG, UK

[23] Neurology Unit, Department of Pediatrics, Faculty of Medicine, University of Alexandria, Alexandria, Egypt

[24] Department of Family Health, High Institute of Public Health, Faculty of Medicine, University of Alexandria, Alexandria, Egypt

[25] Department of Biotechnology and Genetic Engineering, Philadelphia University, Amman 19392, Jordan

[26] Provincial Medical Genetics Program at BC Women's Health Centre, Vancouver, BC V6H 3N1, Canada

[27] Department of Neurosciences, University of California San Diego, La Jolla, CA, USA

[28] Rady Children's Institute for Genomic Medicine, San Diego, CA, USA

[29] Department of Pediatric Neurology, Indira Gandhi Institute of Child Health, Bangalore, India

[30] Center for Neurology and Hertie Institute for Clinical Brain Research, University Tübingen, Tübingen 72076, Germany

[31] German Center of Neurodegenerative Diseases (DZNE), Tübingen 72076, Germany

[32] Southern California Kaiser Permanente Medical Group, Department of Regional Genetics, Anaheim, CA 92806, USA

[33] Madigan Army Medical Center, Tacoma, WA 98431, USA

[34] Department of Paediatrics and Child Health, University of Otago, Wellington, 6242, New Zealand

[35] Molecular and Clinical Sciences Institute, St. George's, University of London, Cranmer Terrace, London SW17 0RE, UK

[36] Department of Medical Genetics, Next Generation Genetic Polyclinic, Mashhad, Iran

[37] Department of Neuropediatrics, University Children's Hospital, Klinikum Oldenburg, Oldenburg 26133, Germany

[38] Division of Genetics and Genomics, Boston Children's Hospital, Boston, MA 02115, USA

[39] 3billion, Inc, Seoul, South Korea

[40] Human Genome Sequencing Center, Baylor College of Medicine, Houston, TX, USA

[41] Cortica Healthcare, San Rafael, CA 94903, USA

[42] GeneDx, Gaithersburg, MD 20877, USA

[43] Centre for Applied Genomics, Genetics, and Genome Biology, Hospital for Sick Children, Toronto, ON M5G 0A4, Canada

[44] UT Southwestern Medical Center, Departments of Pediatrics and Neurology, Dallas, TX 75390, USA

[45] Department of Pediatrics, McGovern Medical School at the University of Texas Health Science Center at Houston (UTHealth) and Children's Memorial Hermann Hospital, Houston, TX 77030, USA

[46] Practice of Human Genetics, Homburg (Saar), Germany

[47] Children's Hospital of Eastern Ontario Research Institute, University of Ottawa, Ottawa K1H 8L1, Canada

[48] Center for Pediatric Genomic Medicine Children's Mercy - Kansas City, Missouri, USA

[49] University of Health Sciences, Zubeyde Hanim Research and Training Hospital of Women's Health and Diseases, Department of Medical Genetics, Ankara 06080, Turkey

[50] Human Genetics and Genome Research Division, Clinical Genetics Department, National Research Centre, Cairo, Egypt

[51] Department of Pharmacology & Therapeutics and Centre de Recherche en Biologie Structurale, McGill University, Montréal, QC H3G 1Y6, Canada

[52] Department of Human Genetics, McGill University, Montréal, QC H3A 2B4, Canada

[53] Division of Neuroradiology, The Children's Hospital of Philadelphia, Philadelphia, PA 19104, USA

[†] The full list of authors in network is in Supplementary Notes.

Abstract

Developmental and epileptic encephalopathies (DEE) are a heterogenous group of epilepsies in which altered brain development can lead to developmental delay and seizures, with the epileptic activity further negatively impacting neurodevelopment[1]. Identifying the underlying cause of DEE is essential for progress towards precision therapy. Here we describe a group of patients with DEE that exhibit a unique cluster of neuroanatomical signatures due to biallelic variants in *DENND5A*. We demonstrate that DENND5A interacts with MUPP1 and PALS1, components of the Crumbs apical polarity complex, which is required for both neural progenitor cell identity and the ability of these stem cells to divide symmetrically[2]. Induced pluripotent stem cells lacking *DENND5A* fail to undergo symmetric cell division during neural induction and have an inherent propensity to differentiate into neurons. Similarly, transgenic *DENND5A* mice, with phenotypes consistent with the human syndrome, have an increased number of neurons in the

proliferative adult subventricular zone. Disruption of symmetric cell division following loss of *DENND5A* results from misalignment of the mitotic spindle in apical neural progenitors, an observation also observed in PALS1 null zebrafish embryos[3]. This orients cells away from the proliferative apical domain surrounding the ventricles, biasing daughter cells towards a more fate-committed state, and ultimately halting neurodevelopment. This study provides a mechanism behind *DENND5A*-related DEE that may also be generalizable to other developmental conditions and provides variant-specific clinical information for physicians and families.

Main Text

Developmental and epileptic encephalopathies (DEE) are characterized by developmental delay and drug-resistant seizures. Abnormal neurodevelopmental outcomes are the result of both the underlying etiology and the negative impact of frequent epileptic activity on the developing brain[1]. Homozygous variants in *DENND5A* (DENN Domain Containing protein 5A), a gene encoding a protein expressed at high levels in the developing brain, have previously been linked to DEE[4,5], but the function of the protein during development is unknown. We now determine that DENND5A interacts with MUPP1/PALS1, apical polarity proteins involved in cell division and neurodevelopment. Consistently, perturbations in genes related to cell division and polarity are associated with developmental defects consistent with DEE[6-11].

Proteins comprising the apical membrane-defining Crumbs (Crb) complex in neuroepithelia include CRB2, MUPP1 (Multi-PDZ Protein 1, also known as MPDZ) or PATJ (Pals1-Associated Tight Junction Protein), and PALS1 (Protein Associated With Lin7 1) and have been extensively studied in their roles in cell polarization and tissue development[12,13]. Most research on the Crb complex focuses on the version of the complex containing PATJ rather than MUPP1, and the only study directly comparing the function of the two highly similar proteins concludes that PATJ is essential but MUPP1 is dispensable for establishing and maintaining tight junctions (TJs)[14]. *Ex vivo* studies, however, reveal significant deficits in ependymal[15,16] and choroid plexus epithelial cells[17] upon loss of MUPP1, including a complete loss of PALS1 expression in ependymal cells of *MUPP1* KO mice[16]. Although ependymal cells do not have TJs[18] or stem cell properties[19], they derive from TJ-containing neuroepithelial cells that gradually transition into radial glial cells that rely on sparse TJ and abundant adherens junction (AJ) protein expression to

maintain their progenitor identity and ability to divide symmetrically[2,20-22]. Indeed, MUPP1 may differ from PATJ in that it preferentially stabilizes AJs over TJs[14].

We have identified a cohort of 23 individuals from 21 families with biallelic *DENND5A* variants and determined their clinical presentation through a phenotypic survey answered by their treating clinicians, coupled with MRI analysis. Severe cases show a cluster of neuroanatomical hallmarks unique to this form of DEE: microcephaly, ventriculomegaly, calcifications, diencephalic-mesencephalic junction dysplasia, pontocerebellar hypoplasia, and dysgenesis of the basal ganglia, corpus callosum and cerebral cortex, the latter particularly due to evidence of pachygyria in the occipital lobes. To gain insight on the function of DENND5A, we employed mouse and zebrafish models of *DENND5A*-related DEE and *DENND5A* knockout (KO) induced pluripotent stem cells (iPSCs) and determined that DENND5A is essential for apical neural progenitor cell self-renewal during neurodevelopment.

Phenotypic overlap in individuals with biallelic *DENND5A* variants

Our cohort for phenotypic analysis consisted of 23 people (12 F, 11 M, mean age = 8.2 years, *SD* = 5.3) from 21 families with biallelic *DENND5A* variants. Twenty-eight unique *DENND5A* variants were identified across the 14 homozygous and 9 compound heterozygous individuals. Seven members of the cohort were reported to have at least one additional variant flagged as potentially causative. Extended Data Table 1 summarizes each person in the cohort, including their participant IDs, gene variant(s), predicted American College of Medical Genetics and Genomics variant interpretations, allele frequencies obtained from the gnomAD v2.1.1 dataset (https://gnomad.broadinstitute.org), brain abnormalities, and developmental outcomes. Pedigrees are available in Extended Data Figure 1 for participants 25-28, and some have affected family members not included in the cohort due to the unavailability of their clinical data. Pedigrees for participants 10, 15, and 16 were published previously[4]. None of the *DENND5A* point mutations in the cohort were found in the homozygous state among 140,000 individuals on gnomAD, a database that removes individuals affected by severe pediatric disease, indicating that biallelic pathogenic variants are likely incompatible with normal development. Twenty-three of the variants are found in the coding sequence, 2 are copy number variants (exon 1-14 duplication [NC_000011.9:(9171749_9172227)_(9316934_9321244)dup] and exon 1 deletion [NC_000011.10:g. 9262758_9268826del]), and 3 intronic variants are located in splice sites

(splice donor variants c.2283+1G>T and c.949+1G>A, and polypyrimidine tract variant c.950-20_950-17delTTTT). The coding variants span the length of the protein including 9 in the DENN domain, 2 in the RUN1 domain, 4 in the PLAT domain, 4 in the RUN2 domain, and 4 in predicted linker regions between the folded modules (Fig. 1a).

Supplementary Data 1 provides complete phenotypic data for each member of the cohort. The most frequently reported phenotypes observed in individuals with biallelic *DENND5A* variants were global developmental delay (22/23), seizures (20/23), microcephaly (17/23), and ventriculomegaly (14/23; Figure 1b). A majority of cohort members displayed all or most of these clinical features, but it is important to note that participant 19 (p.P955L/p.T136R) exhibited only global developmental delay and did not undergo neuroimaging, and participant 8 (p.K485E/p.R1159W) did not present with any of the four features and had a normal brain MRI, suggesting that these individuals do not have *DENND5A*-related DEE and that one or more of these variants may in fact be benign (Figure 1c). Additionally, although microcephaly was the most prevalent structural abnormality and appears to be a main feature of *DENND5A*-related DEE, occipitofrontal circumference (OFC) percentiles ranged considerably (*Min* = < 1, *Max* = 97) with one case of macrocephaly also reported, possibly secondary to external hydrocephalus (OFC percentiles: *M* = 18.5, *Mdn* = 2.9, *SD* = 30.2).

Failure to meet key developmental milestones was almost universal in the cohort, evidenced by the fact that all but one (participant 8; p.K485E/p.R1159W) presented with global developmental delay. Although the mean age was 8.3 years (*SD* = 5.3, *Min* = 1, *Max* = 18), most (90%) were nonverbal or limited to single-word speech, and eye contact was observed in less than half (43%) of the cohort. Regarding gross and fine motor skill development, 7/23 could walk independently and 10/23 were able to reach for and grasp objects. Seizures were reported in 20/23 individuals, with an average age of onset of 3 months (*SD* = 3.6 months) and ranging from birth to 12 months. Seizures were controlled in 7 cases with variable antiepileptic treatment.

We analyzed DENND5A protein levels in cell lines derived from 5 cohort members: 3 from neural progenitor cells (NPCs) differentiated from induced pluripotent stem cells (iPSCs), and 2 from immortalized lymphoblasts, with homozygous and compound heterozygous as well as frameshift, nonsense, and missense variants represented. NPCs express SOX1, SOX2 and Nestin, affirming their NPC identity (Extended Data Fig. 2). All patient-derived cells exhibit a reduction

or abolishment of DENND5A protein (Fig. 1d-e), indicating disease phenotypes are a result of protein loss of function; however, the KO validated DENND5A antibody recognizes a region of the protein more C-terminal to the stop codon of p.K205X. RT-qPCR was thus performed, but a poor correlation between *DENND5A* mRNA and protein levels was observed as *DENND5A* mRNA expression from patient-derived cells did not differ significantly from controls (Extended Data Fig. 3a-b). This includes NPCs with homozygous p.K850Sfs*11 variants, where the antibody can determine that a ~100 kDa truncated protein is not expressed because its epitope should still be detected, but mRNA levels were comparable to WT NPCs. When introduced into a FLAG-tagged DENND5A plasmid construct and overexpressed in HEK293T cells, p.K205X resulted in no detectable protein, indicating that even if a truncated protein is produced it is rapidly degraded (Extended Data Fig. 3c).

Magnetic resonance images (MRIs) or computed tomography (CT) scans revealed abnormalities in 19 of the 22 cases that underwent imaging. Normal MRIs were reported for participants 8 (p.K485E/p.R1159W) and 20 (homozygous exon 1-14dup). Not all images were made available, but all available images are presented in Figure 2 and Extended Data Figure 4. Raw MRI data from 5 cases and raw CT data from 1 case were analyzed by a pediatric neuroradiologist. Of these cases, two unrelated individuals (participants 5 and 14), both homozygous for *DENND5A* frameshift variants, showed a “complete” phenotype and had a combination of neuroanatomical abnormalities that appear unique to *DENND5A*-related DEE. These include severe dysgenesis of the basal ganglia with an indistinct and dysplastic thalamic transition, diencephalic-mesencephalic junction dysplasia, and cortical malformations, particularly with pachygyria involving the occipital lobes. Additional features include a reduced volume of the white matter with associated striatal and periventricular calcifications and ventriculomegaly, agenesis or severe dysplasia/hypoplasia of the corpus callosum, thin anterior commissure, and variable degrees of pontocerebellar hypoplasia (Fig. 2a-b). CT image analysis of another homozygous individual with severe DEE also showed consistent phenotypes, including a thin corpus callosum, mild volume reduction, and lenticulostriate and periventricular calcifications (Extended Data Fig. 4a). MRIs analyzed from two compound heterozygous cases that exhibited severe DEE showed relatively mild neuroanatomical phenotypes (participants 2 and 18; Fig. 2c-d). Raw MRI data from an additional compound heterozygous case (participant 9) were not available, but isolated images showed mild reduced corpus callosum volume (Extended Data Fig.

4b). Participant 8 with variants p.K485E/p.R1159W, who does not present with DEE, had a normal MRI with only mild inferior cerebellar vermis hypoplasia (Extended Data Fig. 4c), providing further evidence for the benign or less deleterious nature of p.R1159W, but not p.K485E, since the latter was found in a child with severe DEE and mild neuroanatomical phenotypes (participant 2, p.K485E/p.R710H; Fig. 2c).

Distinct radiological features found in severe *DENND5A*-related DEE cases

When comparing the combinations of neuroanatomical signatures found in *DENND5A*-related DEE cases with other similar developmental conditions, key differences were noted that point toward a unique genotype-phenotype relationship. A study examining fetuses with diencephalic-mesencephalic junction dysplasias accompanied by developmental ventriculomegaly co-presented with corpus callosum dysgenesis and pontocerebellar hypoplasia, but no microcephaly was reported and their ventriculomegaly was associated with hydrocephalus due to aqueductal stenosis, a feature not identified in our cohort[23]. There is also a considerable degree of phenotypic overlap between our cohort and one comprised of patients with pathogenic *protocadherin-12* variants, but none of the latter patients displayed occipital lobe pachygyria or cerebellar hypoplasia as observed here[7]. Gyral simplification and calcifications are observed in cases with recessive variants in the tight junction protein-encoding *OCLN* gene, but severe basal ganglia or diencephalic and mesencephalic dysplasias were not reported and polymicrogyria, a key feature of *OCLN* mutations, is not observed in our study[6]. Variants in tubulin genes also result in overlapping phenotypes[24], but our cases lack the classic dysgyria pattern and instead are typically observed in the context of occipital pachygyria and differ in that our cases are associated with calcifications. Moreover, it seems that our cases have more severe basal ganglia abnormalities when compared with the typical imaging presentations associated with *TUBA1A*, *TUBB2A*, *TUBB2B*, *TUBB3*, and *TUBG1*[25-27]. Variants in *LIS1*, encoding a protein involved in neuronal migration, results most frequently in a posterior gradient of lissencephaly, without calcifications, and variable degrees of corpus callosum size including thin, normal, and thicker than normal tracts[28,29]. In contrast, corpus callosum volumes were either normal, reduced, or absent with no cases of increased volume in our cohort. Finally, there is a selective involvement of the cortex added to the presence of periventricular calcifications, a unique feature that brings cytomegalovirus-induced brain malformations into the differential but aligns with pseudo-

TORCH syndrome diagnostic criteria in the absence of congenital infection[30,31]. The specific combination of neuroanatomical features that we report in severe cases appears unique. Radiological findings combined with clinical information in Extended Data Table 1 and Supplementary Data 1 provide physicians with valuable information to communicate with families and treatment teams on a case-by-case basis.

Characterization of *DENND5A*-related DEE animal models

We established animal models in mice and zebrafish to study how biallelic pathogenic *DENND5A* variants affect development. A knock-in (KI) mouse model, homozygous for a frameshift variant (c.517_517delGA/p.D173Pfs*8) found in the proband of *DENND5A*-related DEE[4] (participants 15 and 16) and conserved in mice (Extended Data Fig. 6a-b), exhibits anatomical and functional phenotypes consistent with those found in our human cohort. Immunoblotting indicated that full-length DENND5A protein is not expressed in KI mice (Fig. 3a); however, the validated DENND5A antibody has an epitope recognizing a region more C-terminal to the stop codon 8 amino acids past D173. RT-qPCR revealed a significant reduction in expression of *DENND5A* mRNA in KI mouse brains compared to WT (M_{WT} = 1.0, M_{KI} = 0.67, SD_{WT} = 0.68, SD_{KI} = 0.42, two-tailed Welch's $t(13.4) = 2.20$, $p = 0.046$; Fig. 3b), suggesting nonsense-mediated RNA decay. Moreover, DENND5A protein containing the mutation and tagged at the N-terminus with FLAG is degraded when overexpressed in HEK-293T cells (Extended Data Fig. 3c), indicating that even if translated, the protein is degraded. *In vivo* 7T MRI scans revealed that *DENND5A* KI mice have significantly enlarged lateral ventricles (M_{WT} = 4.8 mm^3, M_{KI} = 6.6 mm^3, SD_{WT} = 1.3, SD_{KI} = 2.4, two-tailed Mann-Whitney U, $Z = -2.117$, $p = .034$), consistent with ventriculomegaly (Fig. 3c-d). KI mice also had lower mean and median relative brain sizes, but like our human cohort in which occipitofrontal circumference percentiles varied considerably, a high degree of variability was observed in the mice and the difference did not reach statistical significance (Fig. 3e). Finally, while spontaneous seizures were not observed in the KI mice, they show increased seizure susceptibility compared to WT when administered the potassium channel blocker 4-aminopyridine (M_{WT} = 23.60, M_{KI} = 11.67, SD_{WT} = 2.97, SD_{KI} = 7.20, two-tailed $t(9) = 3.445$, $p = 0.007$; Fig 3f).

A zebrafish model system was also developed to study DENND5A during development. *dennd5a* mRNA was detected throughout embryonic development beginning from the first hour

post-fertilization (hpf) (Extended Data Fig. 5c), and in situ hybridization revealed *dennd5a* expression at the two-cell stage (Fig. 3g). The mRNA was enriched in the central nervous system, retinal ganglion cells (RGCs), the sensory epithelium (otic vesicle, Ov), pharyngeal cephalic musculature (Cm), and the heart (H), as detected 24, 48, and 72 hpf (Fig. 3h-j). Biallelic mutations in *dennd5a* were introduced into zebrafish larvae using CRISPR/Cas9 (F_0 knock-outs [KOs]). Successful KO was confirmed by measuring *dennd5a* mRNA via RT-qPCR compared to Cas9 protein-injected controls (Extended Data Fig. 5d). F_0 KOs show structural and behavioral perturbations consistent with *DENND5A*-related DEE including reduced head size and increased ventricle size (Fig. 3k-n). Moreover, the fish display behavioral phenotypes indicating neurological deficits, including altered locomotor activity during periods of light and dark and reductions in visual and acoustic startle responses (Extended Data Fig. 5e-h). Eye size is also reduced in F_0 KOs (Extended Data Fig. 5i). Taken together, DENND5A has highly conserved functions during development.

DENND5A interacts with protein components of apical polarity Crumbs complex

To better understand molecular mechanisms regulating DENND5A function, we screened for binding partners using affinity purification with multiple regions and domains of DENND5A as bait. Mass spectrometry of purified proteins revealed members of the Crb polarity complex, MUPP1 and PALS1, as major DENND5A binding partners, with the interaction mediated via a GST-tagged peptide flanking the missense variant R710H (Fig. 4a-b). This interaction was confirmed with overexpressed proteins in HEK293T lysate (Fig. 4c).

We analyzed the predicted structure of DENND5A from AlphaFold[32,33] and noted that residues R701, E707, H708, R710, and R716 involved in the interaction with the polarity proteins make hydrogen bonds with residues S10-A11, R273, R129, D598, and R716 of the DENN domain (Fig. 4d), respectively, suggesting a conformational change may be necessary to expose the binding site for MUPP1/PALS1. In fact, full-length DENND5A has limited interaction with these proteins (Fig. 4g). Because DENN domains are evolutionarily conserved protein modules that function as guanine nucleotide exchange factors for Rab GTPases[34], we aligned the co-crystal structure of DENND1B and Rab35 with the predicted DENND5A structure and found that the predicted Rab enzymatic site in DENND5A is blocked by interactions between the DENN and RUN1 (RPIP8, UNC-14 and NESCA)/PLAT (Polycystin-1, Lipoxygenase, Alpha-

Toxin) domains (PDB: 3TW8[35]; Extended Data Fig. 6a). In contrast, a conformational change is not necessary for the known DENND5A effector GTP-Rab6 to bind to the RUN1 domain (PDB: 3CWZ[36]; Extended Data Fig. 6b), suggesting that two functional conformations are both possible and necessary.

We next examined the intramolecular interactions blocking MUPP1/PALS1 binding in the AlphaFold structure of DENND5A and observed a cluster of highly charged residues at the interface of the DENN and RUN1 domains (Fig. 4e), suggesting that the structure can be biochemically manipulated to expose both the Rab and Crb complex binding sites. To confirm this intramolecular interaction experimentally, we performed a pull-down assay with the GST-RUN1/PLAT domains as bait in HEK293T lysate expressing either full-length FLAG-tagged DENND5A or the isolated DENN domain (aa1-680). Both DENND5A constructs bind the RUN1/PLAT domain, with a slightly stronger interaction with the isolated DENN domain (Fig. 4f). Moreover, the DENN domain interaction was impeded with charge masking from higher salt concentrations (Extended Data Fig. 6c). We then performed mutagenesis experiments targeting residues involved in the intramolecular interaction. Mutating E379 resulted in a weak but present interaction between full-length DENND5A and Crb complex proteins, implying that DENND5A molecules were slightly skewed toward an open conformation (Fig. 4g). R710H is predicted to result in the loss of a salt bridge to D598 of the DENN domain, potentially destabilizing the closed structure (Extended Data Fig. 6d). Interestingly, GFP-DENND5A_R710H bound MUPP1-FLAG but did not result in an appreciable increase in PALS1-FLAG binding (Fig. 4g). The weak strength of the interaction between open DENND5A and the apical polarity proteins may indicate that this occurs transiently in cells or only under specific circumstances. Indeed, the conformation-dependent nature of the interaction reflects the importance of these proteins remaining separate from each other under steady state conditions. The biologically relevant mechanism for opening the DENND5A structure remains elusive, but possible candidates include posttranslational modifications or other currently unidentified protein-protein interactions.

The distinction of DENND5A as a polarity-related protein is consistent with clinical observations published previously. Human cases with pathogenic variants in *CRB2* and *MUPP1* have been identified and exhibit ventriculomegaly and corpus callosum dysgenesis[8,9,15,37,38], and

patients with *PALS1* variants show global developmental delay, microcephaly, and sometimes seizures[10]. Moreover, the phenotypes observed in our *DENND5A*-related DEE mouse model are consistent with those found in other mouse models targeting apical polarity proteins. *MUPP1* KO mice have enlarged lateral ventricles[17] and the cortex in *PALS1* conditional KO mice, where PALS1 was selectively depleted from cortical progenitors, fails to develop, thus leading to microcephaly[2].

Loss of DENND5A drives premature neuronal differentiation

Microcephaly in *PALS1* conditional KO mice is due to neural progenitors prematurely exiting the cell cycle and undergoing asymmetric neurogenic cell divisions instead of symmetric proliferative divisions, resulting in the depletion of the progenitor pool and premature neuronal differentiation[2]. We thus tested if DENND5A regulates cell division and differentiation phenotypes. We observed that *DENND5A* KO NPCs grow slower than WT (Fig. 5a). Interestingly, a significant difference was observed even after 24 hours (M_{WT} = 710, M_{KO} = 621, SD_{WT} = 108.8, SD_{KO} = 72.4, two-tailed $t(18) = 2.168$, $p = .044$), likely due to an increased number of apoptotic cells observed post-plating. WT NPCs then rapidly increased in number whereas the number of KO NPCs remained relatively stable, producing a significant difference after 48 (M_{WT} = 1008, M_{KO} = 614, SD_{WT} = 135.6, SD_{KO} = 65.30, two-tailed Welch's $t(12.96) = 8.30$, $p < .0001$) and 72 hours (M_{WT} = 1685, M_{KO} = 683, SD_{WT} = 351.6, SD_{KO} = 35.09, two-tailed Mann-Whitney U, $Z = -3.78$, $p < .0001$).

Remarkably, after passaging newly-formed NPCs into neural progenitor maintenance medium, KO NPCs develop β-III tubulin-positive processes with neuronal morphology after one day, something rarely observed in WT NPCs (M_{WT} = 10.67%, M_{KO} = 47.29%, SD_{WT} = 13.5, SD_{KO} = 21.1, two-tailed Mann-Whitney U, $Z = -3.991$, $p < .0001$; Fig. 5b-c). To determine if this premature differentiation phenotype translates to complex organisms lacking *DENND5A*, we examined the adult mouse subventricular zone, a region that normally retains GFAP-positive radial glia-like neural stem cells[39]. KI mice have a significantly higher percentage of post-mitotic neurons expressing NeuN compared to WT (M_{WT} = 39.6%, M_{KI} = 58.8%, SD_{WT} = 6.7, SD_{KI} = 6.6, two-tailed $t(10) = -4.981$, $p = 0.001$; Fig. 5d-e). While there is also a reduction in GFAP-positive cells in KI SVZs, it did not reach significance (M_{WT} = 43.3%, M_{KI} = 31.9%, SD_{WT} = 12.3, SD_{KI} =

14.1, two-tailed $t(10) = 1.486$, $p = 0.168$). Our results suggest that DENND5A expression promotes stemness and its loss permits cell cycle exit and premature differentiation.

Loss of *DENND5A* misorients mitotic spindles

When the zebrafish homolog of *PALS1* is depleted from the developing retina, progenitor cells undergo asymmetric oblique cell divisions rather than symmetric horizontal divisions, detach from the apical ventricular surface, and prematurely differentiate[3]. We thus performed a neural rosette formation assay, a polarized *in vitro* model of early neural development, to assess the observed cell division and differentiation phenotypes to determine if the orientation of cell division is affected in *DENND5A* KO cells. WT and *DENND5A* KO iPSCs were plated at low density in neural induction medium and neural rosettes were allowed to form for up to 7 days. After 1 day *in vitro* (DIV), both WT and KO rosettes had maximal OCT4 expression, a marker of pluripotency, which rapidly declined by DIV 3 and was completely abolished by DIV 5 (Extended Data Fig. 7a). Expression of the NPC marker SOX2 was observed after 1 DIV, reached maximal levels at DIV 3, then slightly reduced and stabilized at DIV 5-7 (Extended Data Fig. 7b). This characterization is in line with rosettes generated from both iPSCs and embryonic stem cells using various neural induction protocols[21,40,41]. In general, there were many more WT rosettes formed per coverslip compared to KO. As in the NPC proliferation experiment, this may be due to the large amount of KO cell death observed at DIV 1, reducing the number of stem cells initially available for rosette formation. WT rosettes were considerably denser than KOs, but rosette diameter, lumen area, and lumen perimeter did not differ significantly (Extended Data Fig. 7c-e). PALS1 localized apically in both WT and KO rosettes (Fig. 6a), suggesting DENND5A is not involved in trafficking MUPP1/PALS1 to the apical membrane. However, the axis of cell division in relation to the lumen differed (Fig. 6b). We thus measured the mitotic spindle angle, defined as the angle between the cleavage plane and the nearest apical membrane, considering only cells with normally condensed chromatin and both centrosomes marked by γ-tubulin visible in the same plane. Although this exclusion criteria omitted many cells in WT rosettes dividing symmetrically along the z-plane or above the lumen (Extended Data Fig. 7f) as well as numerous observations of dividing cells with abnormally condensed chromatin in KO rosettes (Extended Data Fig. 7g), the spindle angle among cells dividing within WT ($M = 57.1°$, $Mdn = 65.4°$, $SD = 25.9$) and KO ($M = 26.0°$, $Mdn = 20.1°$, $SD = 19.0$) rosettes differed

significantly according to a two-tailed Mann-Whitney U test ($Z = -7.122$, $p < .0001$; Fig. 6c). An overwhelming majority of KO cells divided with spindle angles <45° (Fig. 6d), indicating that *DENND5A* KO results in increased levels of oblique asymmetric cell divisions and the ability for apical progenitors to self-renew is severely compromised.

Conclusion

Physicians encountering infants and children with all or some of the following should consider genetic screening to examine *DENND5A* as a causal factor: global developmental delay, seizures, microcephaly, ventriculomegaly, reduced white matter volume, calcifications, basal ganglia malformations, abnormalities in the diencephalic-mesencephalic junction, and/or cortical malformations. For families in which one parent is aware they are a carrier of a pathogenic *DENND5A* variant, genetic counselors can recommend the other parent undergo genetic testing. When both parents are carriers, *in vitro* fertilization with preimplantation genetic diagnosis can be offered. However, the presence of *DENND5A* variants of unknown clinical significance does not necessarily equate to a devastating prognosis. 13% of our small cohort do not meet criteria for DEE or even experience seizures; p.R1159W, p.P955L, p.T136R, and/or exon 1-14 duplication may be benign variants or variants that have less impact on development. Additionally, we believe American College of Medical Genetics and Genomics classifications for several variants should be updated to pathogenic or likely pathogenic, especially p.R517W, p.K485E, p.D541G and p.R710H, as these variants are found in individuals with brain abnormalities, severe intellectual disability, infantile seizure onset, and no other flagged gene variants. The identification of additional *DENND5A*-related DEE cases will prove valuable for future clinical and biological studies and thus improved treatment options and prognostic information for health care providers and families.

The conformation-dependent interaction between MUPP1/PALS1 and DENND5A at p.R710 may reflect a molecular mechanism to regulate the balance of symmetric versus asymmetric cell division during development. However, the specific biological context of the interaction between DENND5A and MUPP1/PALS1 remains to be identified. Future work should emphasize the mechanisms regulating the DENND5A and MUPP1/PALS1 interaction and identification of its role during cell division. Additionally, we have tested all commercial antibodies against DENND5A using several *DENND5A* KO cell lines and did not observe a specific signal via

immunofluorescence, so the localization of endogenous DENND5A during cell division of apical progenitors is unknown. One can speculate that DENND5A is involved in properly positioning centrosomes to align them parallel to the apical membrane during mitosis, ensuring that both daughter cells inherit apical determinants and remain in contact with the stem and progenitor cell biochemical niche found in the developing ventricle. This is consistent with the apical membrane of neural rosettes being enriched in both cell junctional proteins as well as Golgi-associated proteins[21,41,42], as DENND5A is a Golgi-localized protein[43] and the Golgi is confined to the apical process of apical progenitors in punctate stacks rather than a ribbon structure[44,45]. Golgi fragments containing DENND5A bound to PALS1/MUPP1 may thus ensure equal Golgi and AJ protein inheritance in both daughter cells of a dividing apical progenitor, affecting the resulting daughter cell fates.

Our study provides evidence for the involvement of *DENND5A* in two well-known processes implicated in primary microcephaly: centrosome positioning during cell division and premature NPC cell cycle exit and differentiation[46]. We propose a new disease model in which *DENND5A*-related DEE is driven by a significant reduction in symmetric cell divisions during early development due to the misorientation of cells away from the proliferative apical domain of the ventricular zone. This results in an imbalance of signaling molecules from the stem and progenitor cell niche to each daughter cell and biases one toward a more fate-committed state[47], which prematurely halts neurogenesis and leads to microcephaly. The reduced volume of neurons likely leads to compensatory ventriculomegaly, and improperly positioned prematurely-born neurons that do not undergo apoptosis may form aberrant synaptic contacts resulting in seizures that can further adversely affect development.

References

1. Raga S, Specchio N, Rheims S, Wilmshurst JM. Developmental and epileptic encephalopathies: recognition and approaches to care. *Epileptic Disord*. Feb 1 2021;**23**(1):40-52. doi:10.1684/epd.2021.1244

2. Kim S, Lehtinen MK, Sessa A, et al. The apical complex couples cell fate and cell survival to cerebral cortical development. *Neuron*. Apr 15 2010;**66**(1):69-84. doi:10.1016/j.neuron.2010.03.019

3. Yamaguchi M, Imai F, Tonou-Fujimori N, Masai I. Mutations in N-cadherin and a Stardust homolog, Nagie oko, affect cell-cycle exit in zebrafish retina. *Mech Dev*. May-Jun 2010;**127**(5-6):247-64. doi:10.1016/j.mod.2010.03.004

4. Han C, Alkhater R, Froukh T, et al. Epileptic Encephalopathy Caused by Mutations in the Guanine Nucleotide Exchange Factor DENND5A. *Am J Hum Genet*. Dec 1 2016;**99**(6):1359-1367. doi:10.1016/j.ajhg.2016.10.006

5. Anazi S, Maddirevula S, Faqeih E, et al. Clinical genomics expands the morbid genome of intellectual disability and offers a high diagnostic yield. *Mol Psychiatry*. Apr 2017;**22**(4):615-624. doi:10.1038/mp.2016.113

6. O'Driscoll MC, Daly SB, Urquhart JE, et al. Recessive mutations in the gene encoding the tight junction protein occludin cause band-like calcification with simplified gyration and polymicrogyria. *Am J Hum Genet*. Sep 10 2010;**87**(3):354-64. doi:10.1016/j.ajhg.2010.07.012

7. Guemez-Gamboa A, Caglayan AO, Stanley V, et al. Loss of Protocadherin-12 Leads to Diencephalic-Mesencephalic Junction Dysplasia Syndrome. *Ann Neurol*. Nov 2018;**84**(5):638-647. doi:10.1002/ana.25327

8. Al-Dosari MS, Al-Owain M, Tulbah M, et al. Mutation in MPDZ causes severe congenital hydrocephalus. *J Med Genet*. Jan 2013;**50**(1):54-8. doi:10.1136/jmedgenet-2012-101294

9. Tessier A, Roux N, Boutaud L, et al. Bi-allelic variations in CRB2, encoding the crumbs cell polarity complex component 2, lead to non-communicating hydrocephalus due to atresia of the aqueduct of sylvius and central canal of the medulla. *Acta Neuropathol Commun*. Feb 20 2023;**11**(1):29. doi:10.1186/s40478-023-01519-8

10. Sterling N, Duncan AR, Park R, et al. De novo variants in MPP5 cause global developmental delay and behavioral changes. *Hum Mol Genet*. Dec 18 2020;**29**(20):3388-3401. doi:10.1093/hmg/ddaa224

11. Zanotta N, Panzeri E, Minghetti S, et al. A case of a childhood onset developmental encephalopathy with a novel de novo truncating variant in the Membrane Protein Palmitoylated 5 (MPP5) gene. *Seizure*. Jan 23 2023;doi:10.1016/j.seizure.2023.01.015

12. Assemat E, Bazellieres E, Pallesi-Pocachard E, Le Bivic A, Massey-Harroche D. Polarity complex proteins. *Biochim Biophys Acta*. Mar 2008;**1778**(3):614-30. doi:10.1016/j.bbamem.2007.08.029

13. Tepass U, Theres C, Knust E. crumbs encodes an EGF-like protein expressed on apical membranes of Drosophila epithelial cells and required for organization of epithelia. *Cell*. Jun 1 1990;**61**(5):787-99. doi:10.1016/0092-8674(90)90189-l

14. Adachi M, Hamazaki Y, Kobayashi Y, et al. Similar and distinct properties of MUPP1 and Patj, two homologous PDZ domain-containing tight-junction proteins. *Mol Cell Biol*. May 2009;**29**(9):2372-89. doi:10.1128/MCB.01505-08

15. Saugier-Veber P, Marguet F, Lecoquierre F, et al. Hydrocephalus due to multiple ependymal malformations is caused by mutations in the MPDZ gene. *Acta Neuropathol Commun*. May 1 2017;**5**(1):36. doi:10.1186/s40478-017-0438-4

16. Feldner A, Adam MG, Tetzlaff F, et al. Loss of Mpdz impairs ependymal cell integrity leading to perinatal-onset hydrocephalus in mice. *EMBO Mol Med*. Jul 2017;**9**(7):890-905. doi:10.15252/emmm.201606430

17. Yang J, Simonneau C, Kilker R, et al. Murine MPDZ-linked hydrocephalus is caused by hyperpermeability of the choroid plexus. *EMBO Mol Med*. Jan 2019;**11**(1)doi:10.15252/emmm.201809540

18. Serra R, Simard JM. Adherens, tight, and gap junctions in ependymal cells: A systematic review of their contribution to CSF-brain barrier. *Front Neurol*. 2023;**14**:1092205. doi:10.3389/fneur.2023.1092205

19. Shah PT, Stratton JA, Stykel MG, et al. Single-Cell Transcriptomics and Fate Mapping of Ependymal Cells Reveals an Absence of Neural Stem Cell Function. *Cell*. May 3 2018;**173**(4):1045-1057 e9. doi:10.1016/j.cell.2018.03.063

20. Eze UC, Bhaduri A, Haeussler M, Nowakowski TJ, Kriegstein AR. Single-cell atlas of early human brain development highlights heterogeneity of human neuroepithelial cells and early radial glia. *Nat Neurosci*. Apr 2021;**24**(4):584-594. doi:10.1038/s41593-020-00794-1

21. Boroviak T, Rashbass P. The apical polarity determinant Crumbs 2 is a novel regulator of ESC-derived neural progenitors. *Stem Cells*. Feb 2011;**29**(2):193-205. doi:10.1002/stem.567

22. Bendriem RM, Singh S, Aleem AA, Antonetti DA, Ross ME. Tight junction protein occludin regulates progenitor Self-Renewal and survival in developing cortex. *Elife*. Dec 3 2019;**8**doi:10.7554/eLife.49376

23. Severino M, Righini A, Tortora D, et al. MR Imaging Diagnosis of Diencephalic-Mesencephalic Junction Dysplasia in Fetuses with Developmental Ventriculomegaly. *AJNR Am J Neuroradiol*. Aug 2017;**38**(8):1643-1646. doi:10.3174/ajnr.A5245

24. Romaniello R, Arrigoni F, Fry AE, et al. Tubulin genes and malformations of cortical development. *Eur J Med Genet*. Dec 2018;**61**(12):744-754. doi:10.1016/j.ejmg.2018.07.012

25. Hung KL, Lu JF, Su DJ, Hsu SJ, Wang LC. Tubulinopathy Presenting as Developmental and Epileptic Encephalopathy. *Children (Basel)*. Jul 23 2022;**9**(8)doi:10.3390/children9081105

26. Brock S, Vanderhasselt T, Vermaning S, et al. Defining the phenotypical spectrum associated with variants in TUBB2A. *J Med Genet*. Jan 2021;**58**(1):33-40. doi:10.1136/jmedgenet-2019-106740

27. Lee YH, Park NH. A Complex Cortical Malformation Caused by a Mutation in the Tubulin-Encoding TUBB3 Gene. *Taehan Yongsang Uihakhoe Chi*. Sep 2020;**81**(5):1246-1249. doi:10.3348/jksr.2019.0175

28. Saillour Y, Carion N, Quelin C, et al. LIS1-related isolated lissencephaly: spectrum of mutations and relationships with malformation severity. *Arch Neurol*. Aug 2009;**66**(8):1007-15. doi:10.1001/archneurol.2009.149

29. Maillard C, Roux CJ, Charbit-Henrion F, et al. Tubulin mutations in human neurodevelopmental disorders. *Semin Cell Dev Biol*. Mar 15 2023;**137**:87-95. doi:10.1016/j.semcdb.2022.07.009

30. Teissier N, Fallet-Bianco C, Delezoide AL, et al. Cytomegalovirus-induced brain malformations in fetuses. *J Neuropathol Exp Neurol*. Feb 2014;**73**(2):143-58. doi:10.1097/NEN.0000000000000038

31. Vivarelli R, Grosso S, Cioni M, et al. Pseudo-TORCH syndrome or Baraitser-Reardon syndrome: diagnostic criteria. *Brain Dev*. Mar 2001;**23**(1):18-23. doi:10.1016/s0387-7604(00)00188-1

32. Jumper J, Evans R, Pritzel A, et al. Highly accurate protein structure prediction with AlphaFold. *Nature*. Aug 2021;**596**(7873):583-589. doi:10.1038/s41586-021-03819-2

33. Varadi M, Anyango S, Deshpande M, et al. AlphaFold Protein Structure Database: massively expanding the structural coverage of protein-sequence space with high-accuracy models. *Nucleic Acids Res*. Jan 7 2022;**50**(D1):D439-D444. doi:10.1093/nar/gkab1061

34. Marat AL, Dokainish H, McPherson PS. DENN domain proteins: regulators of Rab GTPases. *J Biol Chem*. Apr 22 2011;**286**(16):13791-800. doi:10.1074/jbc.R110.217067

35. Wu X, Bradley MJ, Cai Y, et al. Insights regarding guanine nucleotide exchange from the structure of a DENN-domain protein complexed with its Rab GTPase substrate. *Proc Natl Acad Sci U S A*. Nov 15 2011;**108**(46):18672-7. doi:10.1073/pnas.1110415108

36. Recacha R, Boulet A, Jollivet F, et al. Structural basis for recruitment of Rab6-interacting protein 1 to Golgi via a RUN domain. *Structure*. Jan 14 2009;**17**(1):21-30. doi:10.1016/j.str.2008.10.014

37. Lamont RE, Tan WH, Innes AM, et al. Expansion of phenotype and genotypic data in CRB2-related syndrome. *Eur J Hum Genet*. Oct 2016;**24**(10):1436-44. doi:10.1038/ejhg.2016.24

38. Slavotinek A, Kaylor J, Pierce H, et al. CRB2 mutations produce a phenotype resembling congenital nephrosis, Finnish type, with cerebral ventriculomegaly and raised alpha-fetoprotein. *Am J Hum Genet*. Jan 8 2015;**96**(1):162-9. doi:10.1016/j.ajhg.2014.11.013

39. Liu X, Bolteus AJ, Balkin DM, Henschel O, Bordey A. GFAP-expressing cells in the postnatal subventricular zone display a unique glial phenotype intermediate between radial glia and astrocytes. *Glia*. Oct 2006;**54**(5):394-410. doi:10.1002/glia.20392

40. Zhang XZ, Huo HQ, Zhu YQ, et al. Folic Acid Rescues Valproic Acid-Induced Morphogenesis Inhibition in Neural Rosettes Derived From Human Pluripotent Stem Cells. *Front Cell Neurosci*. 2022;**16**:888152. doi:10.3389/fncel.2022.888152

41. Fedorova V, Vanova T, Elrefae L, et al. Differentiation of neural rosettes from human pluripotent stem cells in vitro is sequentially regulated on a molecular level and accomplished by the mechanism reminiscent of secondary neurulation. *Stem Cell Res*. Oct 2019;**40**:101563. doi:10.1016/j.scr.2019.101563

42. Dreser N, Madjar K, Holzer AK, et al. Development of a neural rosette formation assay (RoFA) to identify neurodevelopmental toxicants and to characterize their transcriptome disturbances. *Arch Toxicol*. Jan 2020;**94**(1):151-171. doi:10.1007/s00204-019-02612-5

43. Miserey-Lenkei S, Waharte F, Boulet A, et al. Rab6-interacting protein 1 links Rab6 and Rab11 function. *Traffic*. Oct 2007;**8**(10):1385-403. doi:10.1111/j.1600-0854.2007.00612.x

44. Taverna E, Huttner WB. The Golgi Apparatus in Polarized Neuroepithelial Stem Cells and Their Progeny: Canonical and Noncanonical Features. *Results Probl Cell Differ*. 2019;**67**:359-375. doi:10.1007/978-3-030-23173-6_15

45. Taverna E, Mora-Bermudez F, Strzyz PJ, et al. Non-canonical features of the Golgi apparatus in bipolar epithelial neural stem cells. *Sci Rep*. Feb 16 2016;**6**:21206. doi:10.1038/srep21206

46. Jean F, Stuart A, Tarailo-Graovac M. Dissecting the Genetic and Etiological Causes of Primary Microcephaly. *Front Neurol*. 2020;**11**:570830. doi:10.3389/fneur.2020.570830

47. Knoblich JA. Mechanisms of asymmetric stem cell division. *Cell*. Feb 22 2008;**132**(4):583-97. doi:10.1016/j.cell.2008.02.007

Figures

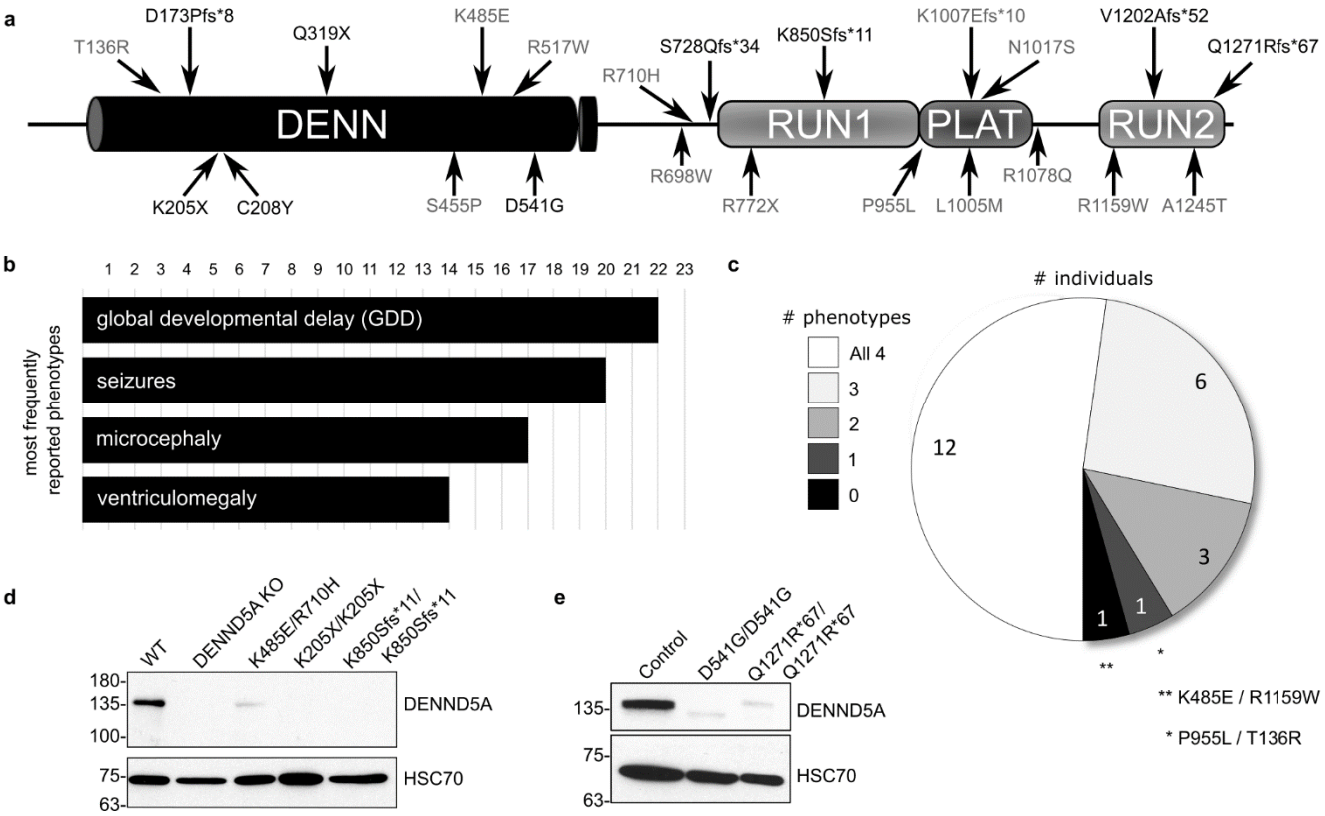

Figure 1: *DENND5A* loss of function variants influence neurodevelopment. a, Schematic of DENND5A protein with all coding sequence variants identified in the study. Black = found in homozygous individuals, gray = found in compound heterozygous individuals. **b,** Number of people with biallelic *DENND5A* variants exhibiting each phenotype. **c,** Number of people with biallelic *DENND5A* variants exhibiting 0, 1, 2, 3, or all 4 of the most frequently reported phenotypes listed in *(b)*. Participant 8 with p.K485E/p.R1159W variants did not present with any phenotype, and the participant 19 with p.955L/p.T136R variants did not undergo neuroimaging but did not have microcephaly or seizures. **d,** Full-length DENND5A protein expression is reduced or abolished in *DENND5A* KO and patient-derived (participants 2, 3, and 10) induced pluripotent stem cells (iPSCs) that were differentiated into neural progenitor cells (NPCs). **e,** Lymphoblasts from two homozygous cases (participants 4 and 5) show reduced DENND5A protein levels compared to lymphoblasts derived from a healthy control. A slight downward band shift from cells derived from the participant 4 with p.D541G variants is consistently observed.

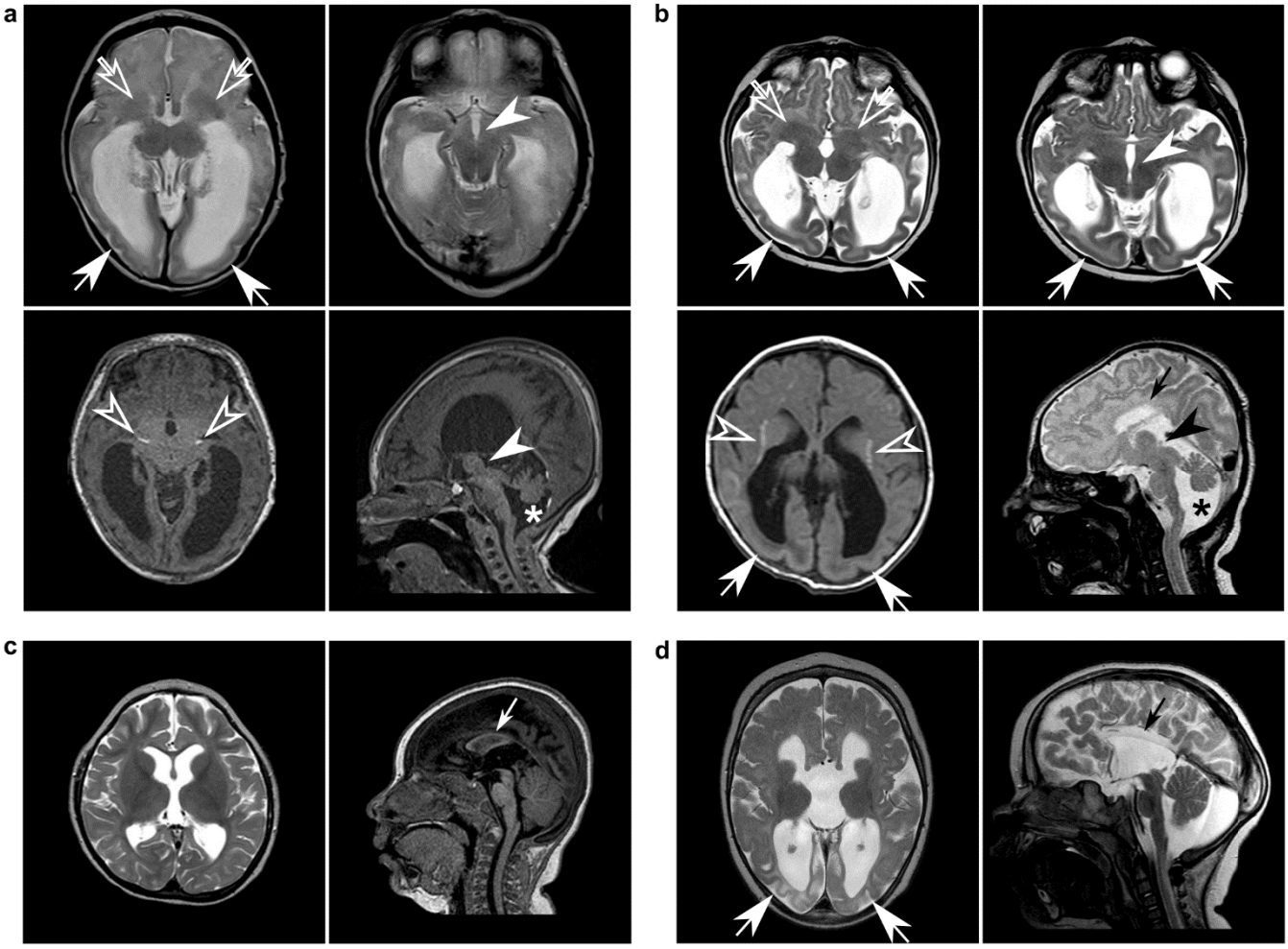

Figure 2: Cortical malformations, corpus callosum and anterior commissure dysgenesis, ventriculomegaly, basal ganglia dysgenesis, calcifications, and diencephalic/mesencephalic dysplasia are indicative of severe *DENND5A*-related DEE. Sample MRI slices from unrelated individuals with **a,** homozygous p.Q1271R*67 variants (participant 5); **b,** homozygous p.S728Qfs*34 variants (participant 14); **c,** compound heterozygous p.K485E/p.R710H variants (participant 2); and **d,** compound heterozygous c.2283+1G>T/p.K1007Efs*10 variants (participant 18) show many neuroanatomical phenotypes in common. Arrows = posterior gradient of pachygyria/lissencephaly; open arrows = severe basal ganglia dysmorphism; arrowheads = diencephalic/mesencephalic junction dysplasia; open arrowheads = periventricular, striatal, and diencephalic calcifications; small arrows = corpus callosum dysgenesis/agenesis; asterisks = cerebellar hypoplasia.

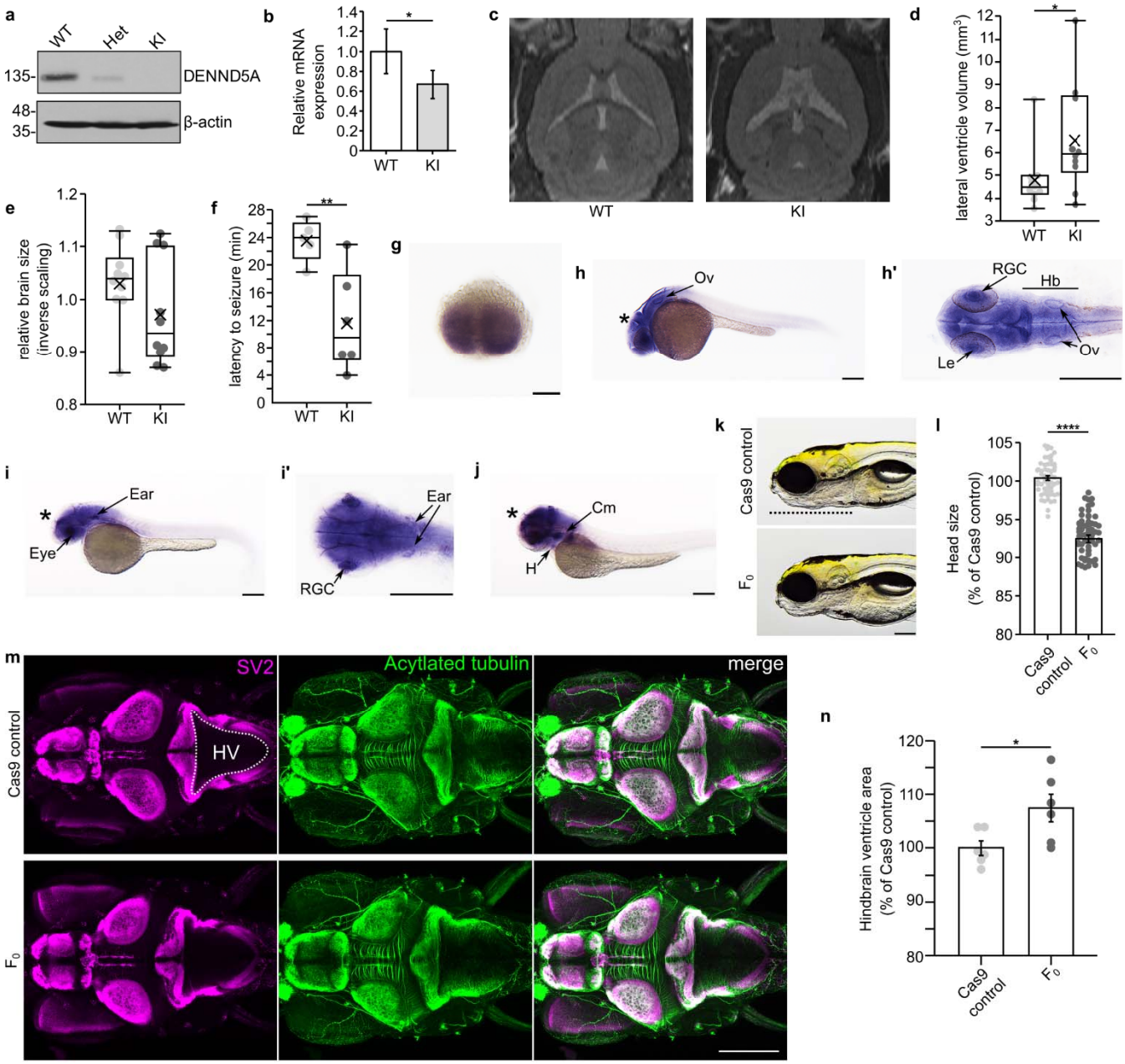

Figure 3: Animal models of *DENND5A*-DEE exhibit common phenotypes observed in the human cohort. a, Mice heterozygous (Het) for p.D173Pfs*8 express full-length DENND5A protein at half the levels compared to WT mice and homozygous knock-in (KI) mice express no full-length DENND5A protein. **b,** Relative brain *DENND5A* mRNA levels measured via RT-qPCR from *n* = 6 total mice. Experiments were performed in triplicate in 3 independent experiments. Error bars = SEM. **c,** Sample images of WT and KI *in vivo* 7T MRIs. **d,** Quantification of pooled lateral ventricle volumes obtained through segmenting *n* = 10 mouse MRIs. **e,** Quantification of relative brain volumes measured using MRI data from *n* = 10 mice

(M_{WT} = 1.03, Mdn_{WT} = 1.04, M_{KI} = 0.97, *MdnKI* = 0.94, SD_{WT} = 0.08, SD_{KI} = 0.10, two-tailed Mann-Whitney U, Z = -1.361, p = .174). **f,** Quantification of seizure latency after injection of 4-AP. Multiple independent experiments were performed with a total of n = 5 WT and n = 6 KI mice. Each dot represents one animal. *(g-j)* Whole-mount *in situ* hybridization shows *dennd5a* mRNA expression at **g,** 0.75 hpf, **h,** 24 hpf, **i,** 48 hpf and **j,** 72 hpf. Asterisks = brain; Ov = otic vesicle; Le = lens; RGC = retinal ganglion cells; Hb = hindbrain; H = heart; Cm = cephalic musculature. Scale bar = 0.2 mm. **k,** Sample images of control and F_0 KO zebrafish head size. Dotted line marks the length of the head used in quantification. Scale bar = 0.2 mm. **l,** Quantification of head size in n = 60 larvae analyzed via two-tailed Mann-Whitney U test (Z = .9.206, p < .0001). Each dot represents one larva. Data are mean ± SEM. **m,** Representative image of larva at 6 dpf immunostained with anti-SV2 (magenta) and anti-acetylated tubulin (green). Dorsal view, anterior to the left. HV = hindbrain ventricle. Dotted line outlines hindbrain ventricle area used in quantification. **n,** Quantification of hindbrain ventricle area in n = 6 larvae analyzed via two-tailed student's t-test (t(10) = , p = 0.028). Data are mean ± SEM. Each dot represents one larva.

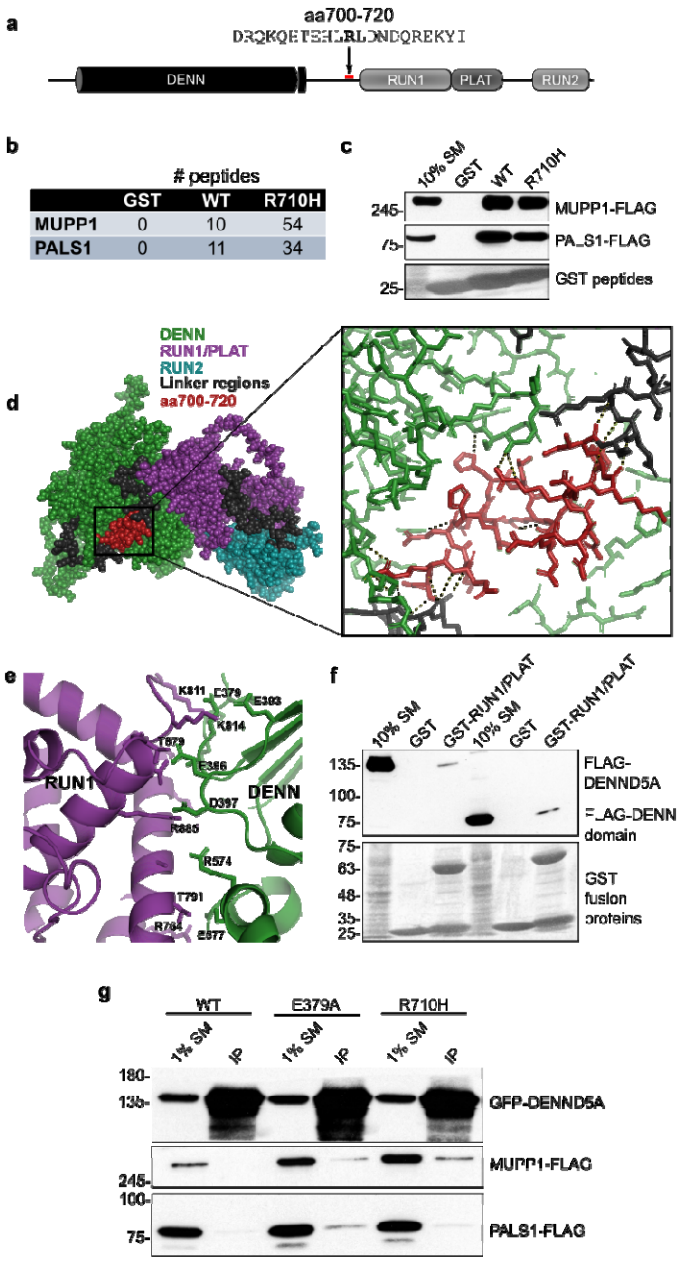

Figure 4: DENND5A interacts with polarity proteins MUPP1 and PALS1. **a,** A recombinant GST-tagged peptide containing amino acids 700-720 of human DENND5A sequence was generated for use in pulldown experiments. The bolded residue corresponds to Arg710 that is affected in the cohort (R710H). **b,** Table indicating the number of peptides corresponding to MUPP1 and PALS1 found bound to each GST fusion peptide used in the pulldown/mass spectrometry experiment. **c,** Overexpressed human MUPP1- and PALS1-FLAG bind to GST-tagged DENND5A peptides. **d,** Residues 700-720 are shown in red in a space-fill model (left) and magnified view (right) of the predicted DENND5A protein structure from AlphaFold. Dotted lines indicate hydrogen bonds. **e,** The interface between the DENN and RUN1 domains of DENND5A comprise many charged residues. **f,** GST pulldown experiments show that FLAG-DENN and GST-RUN1/PLAT physically interact. **g,** Co-immunoprecipitations between GFP-DENND5A and MUPP1- and PALS1-FLAG show that DENND5A only binds the polarity proteins when the intramolecular DENN-RUN1 interaction is disrupted.

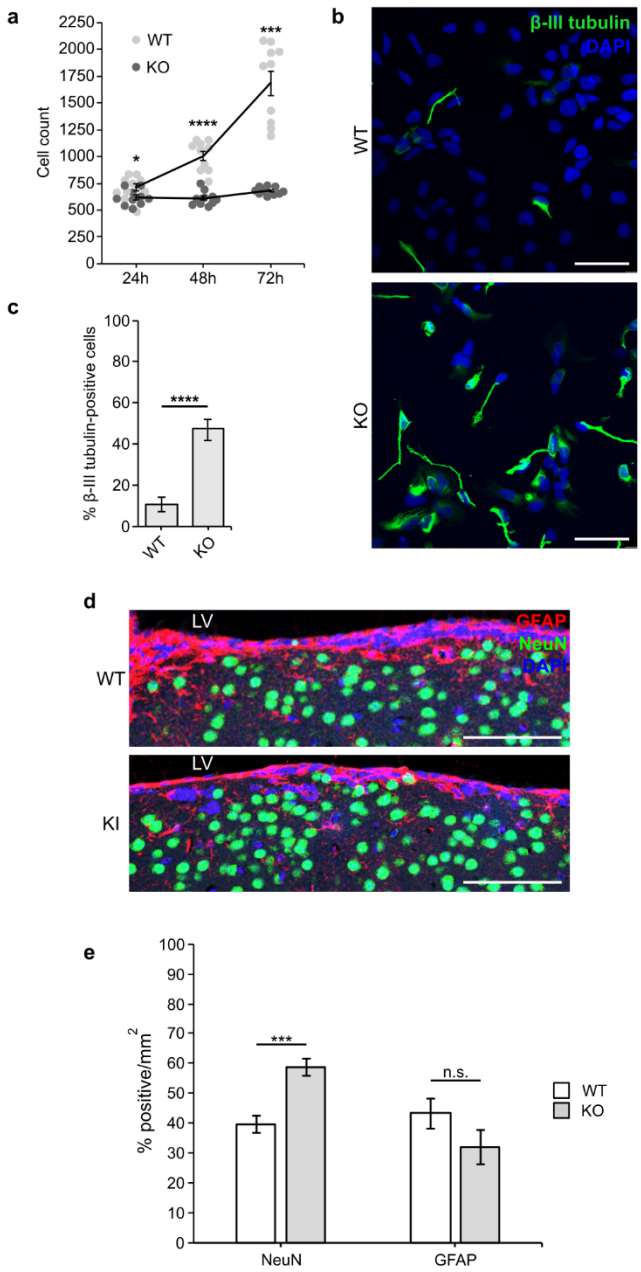

Figure 5: Loss of DENND5A results in premature neuronal differentiation. a, Graph showing the average number of NPCs counted per well of a 96-well plate 24, 48, and 72 hours after plating equal numbers of cells. Data are derived from 10 technical replicates from $n = 2$ independent experiments. Error bars = SEM. **b,** Immunostaining of β-III tubulin (green) and DAPI (blue) in NPCs one day after plating. Scale bar = 50 µm. **c,** Quantification of the percent of β-III tubulin-positive cells per field. A total of $n = 2267$ cells were analyzed from three independent experiments. Data are means ± SEM. **d,** Immunostaining of GFAP (red), NeuN (green), and DAPI (blue) in the SVZ of adult mice. LV = lateral ventricle. Scale bar = 100 µm. **e,** Quantification of the percentage of cells per mm^2 labeled by NeuN or GFAP from a total of $n = 4$ mice. Data are means ± SEM.

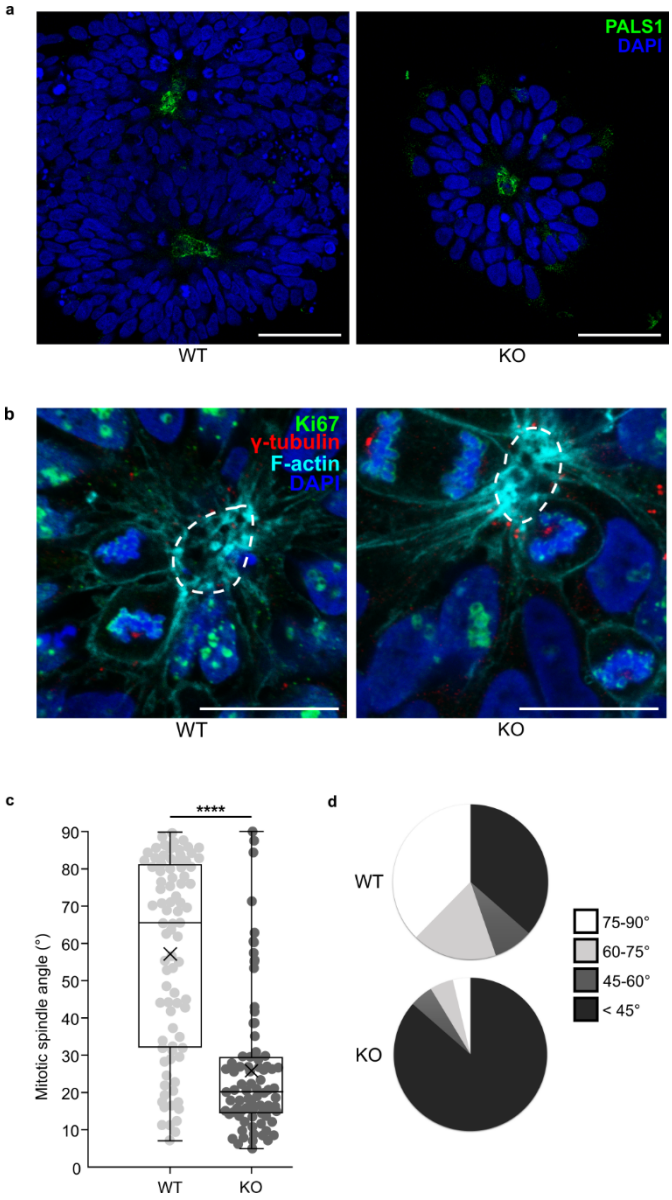

Figure 6: A neural rosette formation assay reveals abnormal mitotic spindle orientations upon loss of *DENND5A*. a, PALS1 staining (green) shows an apical localization in both WT and KO neural rosettes. Scale bars = 50 µm. **b,** Sample images showing the orientation of apical progenitor cell division in WT and *DENND5A* KO rosettes. Green = Ki67, red = γ-tubulin, cyan = F-actin, blue = DAPI. Scale bars = 20 µm. Dotted lines outline the lumen. **c,** Quantification of mitotic spindle angles measured from n = 85 WT and n = 81 KO dividing cells from 2 independent experiments. **d,** Pie charts showing the proportion of dividing cells with mitotic spindle angles falling within various ranges.

ID	Sex, Age Range (years)	*DENND5A* variant(s)	Predicted ACMG classification	Allele frequency	Other gene variants	Seizures	Brain abnormalities	Developmental Outcomes
1	M, 5-10	p.R698W p.N1017S	*VUS* *VUS*	2.78×10^{-5} 1.59×10^{-5}	*CNOT3 (VUS)*	Y	VM	PECS board to communicate, language regression after seizure. ASD and ADHD. Walks independently.
2	F, 5-10	c.1453A>G / p.K485E c.2129G>A / p.R710H	*LB/VUS* *LB/VUS*	7.08×10^{-4} 5.17×10^{-5}	-	Y	Reduced volume, VM, thin CC & AC	Some eye contact, babbles. Can roll over.
3	M, 16-20	c.611_612insG / p.K205X	*LP*	N/A	-	Y	Reduced volume, VM, CH, hemorrhage	No eye contact, speaks in single words. CVI. Walks independently.
4[22]	F, 5-10	c.1622A>G / p.D541G	*VUS*	N/A	-	Y	Thin CC, VM	No eye contact or communication. Can roll over, sits with support.
5[22]	F, 5-10	c.3811del / p.Q1271Rfs*67	*VUS/P*	N/A	-	Y	Reduced volume, posterior gradient of pachygyria/lissencephaly, BG dysmorphism & fusion with thalami, DMD, calcifications, CH, thin CC & AC, VM, hemorrhage	No eye contact or speech. CVI. No motor skills.
7	F, 11-15	c.1363T>C / p.S455P c.3733G>A / p.A1245T	*VUS* *LB/VUS*	N/A 7.96×10^{-6}	*PEX1 (P)*	Y	Periventricular gray matter heterotopias, thin CC & AC, asymmetric lateral ventricles	No eye contact, speaks in single words. Walks with support.
8*	M, 11-15	c.1453A>G / p.K485E c.3475C>T / p.R1159W	*LB/VUS* *VUS*	7.08×10^{-4} 9.20×10^{-5}	*HERC2 (VUS)* *MYBPC3 (P)*	N	Mild cerebellar hypoplasia	Makes eye contact and speaks in sentences. ASD. Walks independently.
9	F, deceased 0-5	c.950-20_950-17delTTTT c.3233G>A / p.R1078Q	*LB* *LB/VUS*	4.06×10^{-5} 2.62×10^{-4}	*TBCK (LB/VUS)*	Y	Reduced volume, thin CC	Used to make eye contact, babble, and grasp objects. Developmental regression after seizure onset. CVI.
10	F, 11-15	c.2547del / p.K850Sfs*11	*P*	N/A	-	Y	Reduced volume, VM, periventricular calcifications, thin CC	Makes eye contact and speaks in single words. ADHD. Walks independently.
12	M, 0-5	c.2314C>T / p.R772X c.3013T>A / p.L1005M	*P* *VUS*	3.19×10^{-5} N/A	CNV: 697 kb gain 6q25.3	Y	Abnormal diffusion suggesting acute ischemia in occipital & posterior parietal regions	No eye contact, speaks in single words. Sits with support.
14	M, 0-5	c.2180dupG / p.S728fs*34	*P*	N/A	-	Y	Reduced volume, VM, posterior gradient of pachygyria/lissencephaly, BG dysmorphism & fusion with thalami, DMD, calcifications, CH, thin CC & AC	No eye contact or speech. CVI. No motor skills.
15[21]	F, 11-15	c.517_518delGA / p.D173Qfs*8	*P*	N/A	-	Y	Reduced volume, VM, CH, BG calcifications, thin CC, arachnoid cyst, asymmetric lateral ventricles	Makes eye contact, babbles. Sits with support and can roll over.
16[21]	F, ?	c.517_518delGA / p.D173Qfs*8	*P*	N/A	-	Y	Reduced volume, VM, CH, BG calcifications, thin CC, asymmetric lateral ventricles	Makes eye contact, babbles. Sits with support.
18	F, 16-20	c.2283+1G>T c.3018dupG / p.K1007Efs*10	*VUS/LP* *LP*	N/A N/A	-	Y	Reduced volume, VM, posterior gradient of pachygyria, BG dysmorphism, CC agenesis, thin AC	No eye contact, babbles. CVI. No motor skills.
19*	M, 5-10	c.407C>G / p.T136R c.2864C>T / p.P955L	*VUS* *VUS*	N/A 1.59×10^{-5}	*CACNA1C (LP/P)*	N	No imaging	Makes eye contact and speaks in sentences. ASD and ADHD diagnoses. Walks independently.
20*	M, 0-5	Exon 1-14 dup	*VUS*	N/A	-	N	None	No eye contact, babbles. Walks with support.
21	M, 16-20	c.1549C>T / p.R517W Exon 1 del	*VUS* *LP*	7.96×10^{-6} N/A	-	Y	Arachnoid cyst	Developmental regression with seizure onset Lost eye contact by 11 months. CVI. Single word at 3 years, nonverbal by 6 years. Walks independently.
22	M, 11-15	c.955C>T / p.Q319X	*P*	N/A	*CDH4 (VUS)*	Y	Reduced volume, VM, thin CC	Makes eye contact. Walks independently.
23	M, 11-15	c.949+1G>A	*LP*	N/A	-	Y	Reduced volume, CH	No eye contact, babbles. CVI. No motor skills.
25	F, 0-5	c.3605del/p.V1202Afs*52	*LP*	N/A	-	Y	Reduced volume, VM, CH, lenticulostriate and periventricular calcifications, thin CC	Developmental regression after seizures. No eye contact or speech. No motor skills.
26	M, 0-5	c.623G>A / p.C208Y	*VUS*	N/A	-	Y	None	Makes eye contact and speaks in single words. Walks independently.
27	M, 0-5	c.949+1G>A	*LP*	N/A	-	Y	Reduced volume, VM, CH	No eye contact or speech. CVI. No motor skills.
28	F, 0-5	c.949+1G>A	*LP*	N/A	-	Y	Reduced volume, VM, CH	No eye contact or speech. CVI. Can roll over and sit with support.

* = no DEE phenotype

LB = Likely Benign
VUS = Variant of Uncertain Significance
LP = Likely Pathogenic
P = Pathogenic

VM = Ventriculomegaly
CC = Corpus Callosum
AC = Anterior Commissure
BG = Basal Ganglia
CH = Cerebellar Hypoplasia
DMD = Diencephalic/Mesencephalic Dysplasia

CVI = Cortical Visual Impairment

Extended Data Table 1: Cohort table indicating demographics, variant details with American College of Medical Genetics and Genomics classifications predicted by Franklin/Varsome software and allele frequencies obtained from gnomAD, and phenotype summaries for each individual in the study.

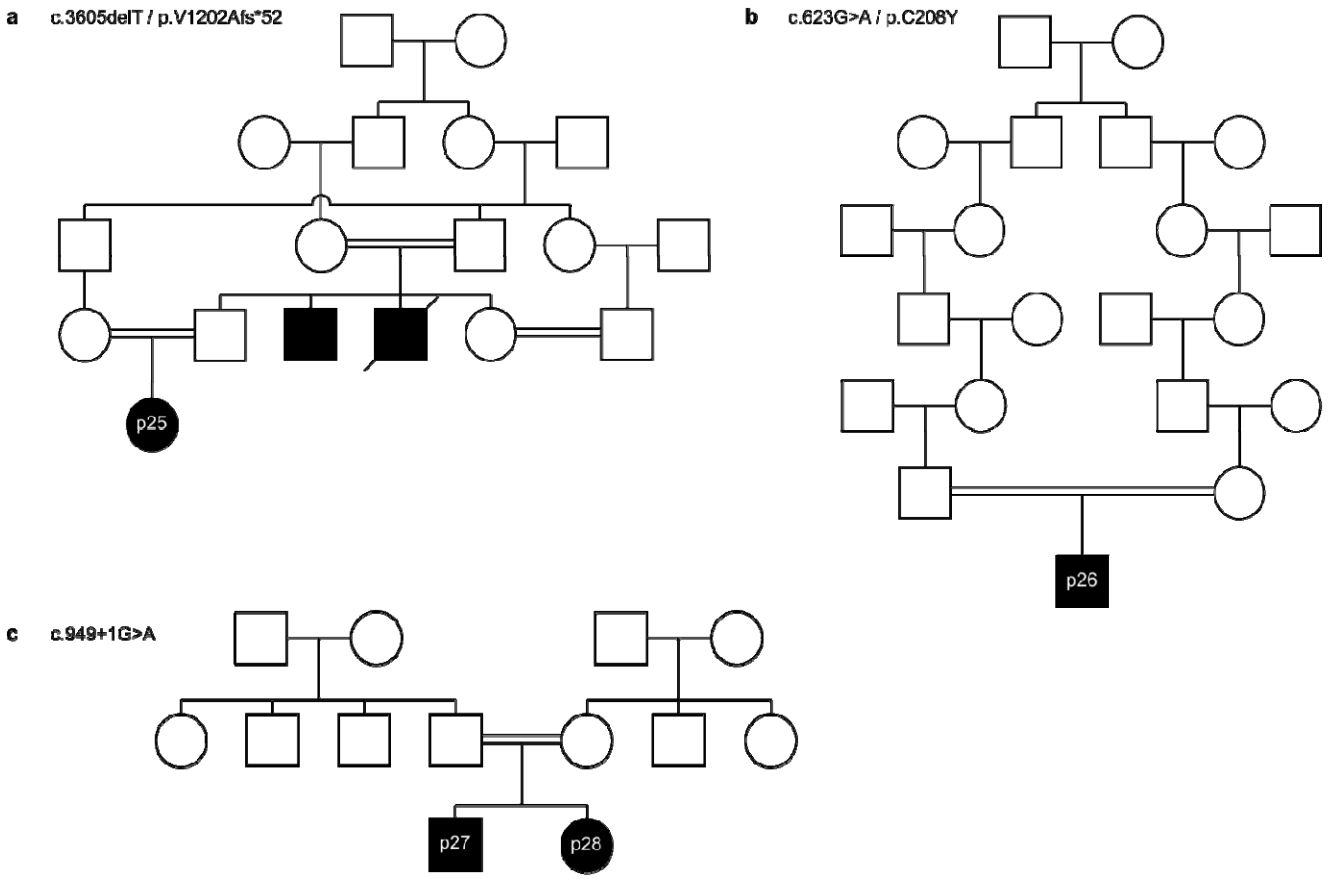

Extended Data Figure 1: Extended pedigrees of consanguineous families demonstrate pathogenicity of select *DENND5A* variants. Pedigrees indicate affected (colored in) and unaffected (open) individuals in families carrying the variants **a,** c.3605delT/p.V1202Afs*52; **b,** c.623G>A/p.C208Y, and **c,** c.949+1G>A. Participants involved in the phenotypic study are indicated by their ID number.

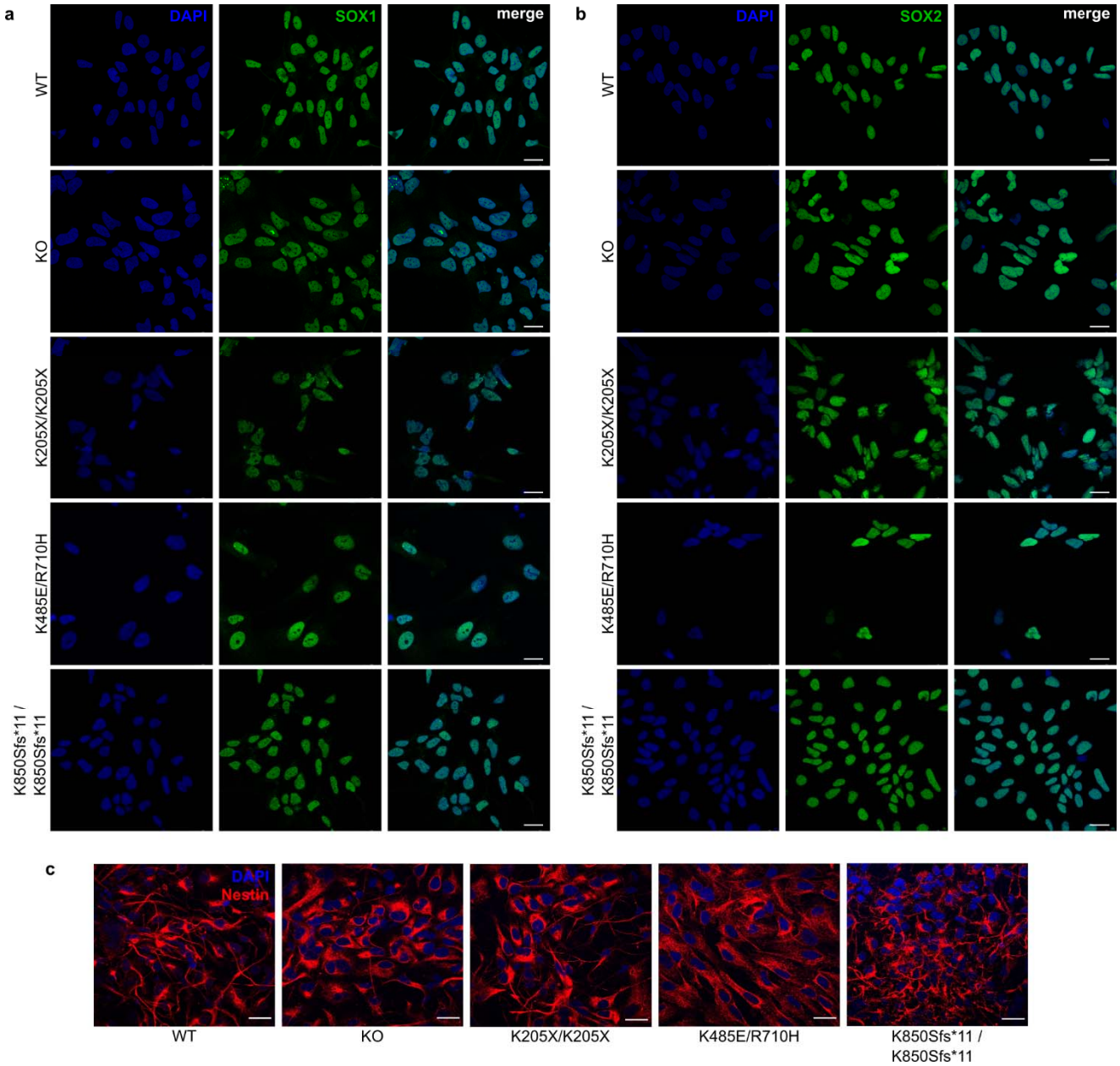

Extended Data Figure 2: All established NPC lines express neural progenitor-specific markers. iPSCs differentiated into NPCs express **a,** SOX1 (green); **b,** SOX2 (green), and **c,** Nestin (red). Blue = DAPI. Scale bars = 20 µm.

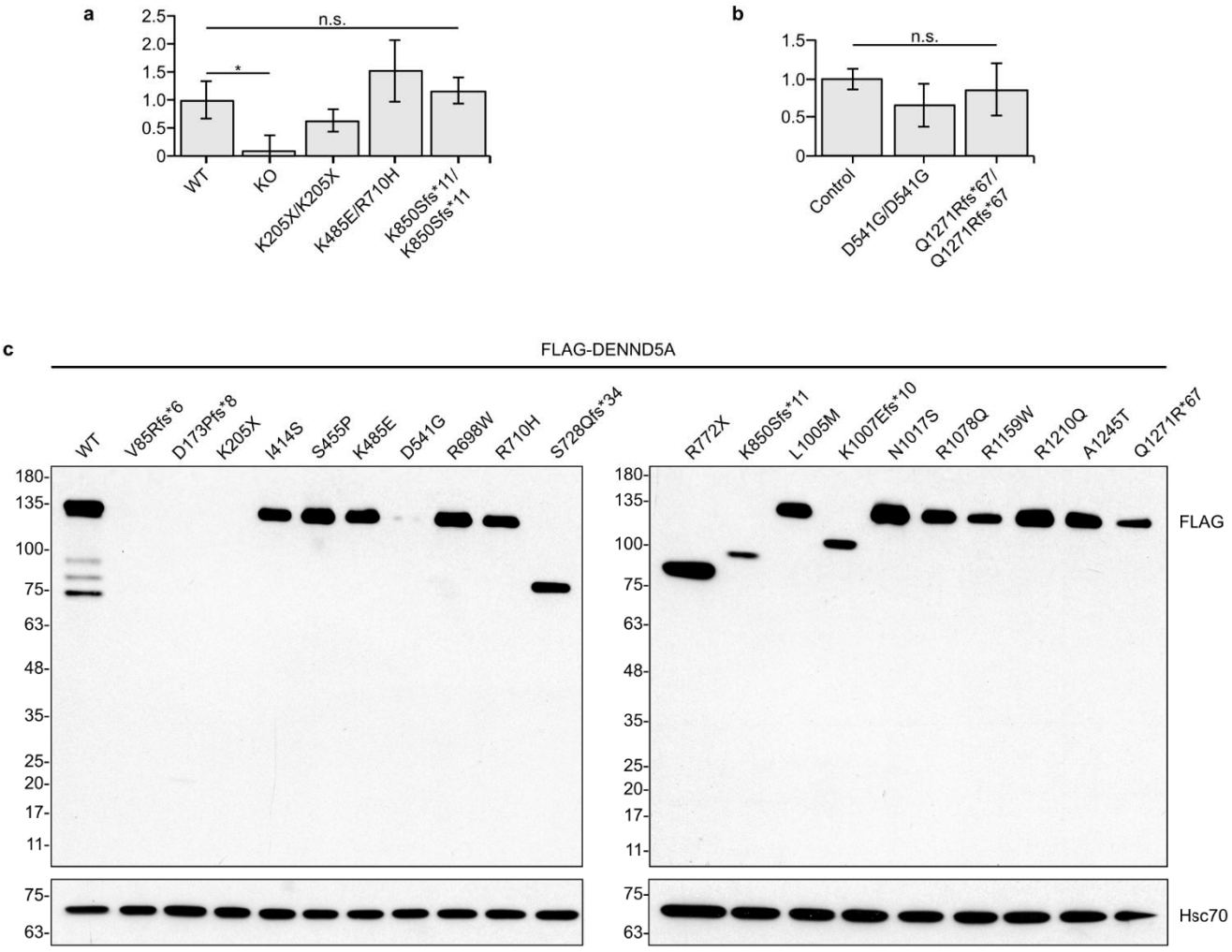

Extended Data Figure 3: DENND5A expression varies depending on the variant. Relative *DENND5A* mRNA expression measured by RT-qPCR in **a,** NPCs and **b,** lymphoblasts. Measurements were made with 4 technical replicates on $n = 3$ independent samples. Data are mean ± SEM analyzed via Kruskal-Wallis tests with Bonferroni-corrected pairwise comparisons. **c,** Overexpression of FLAG-DENND5A mutagenized to contain several variants influences protein stability and expression levels in HEK293T.

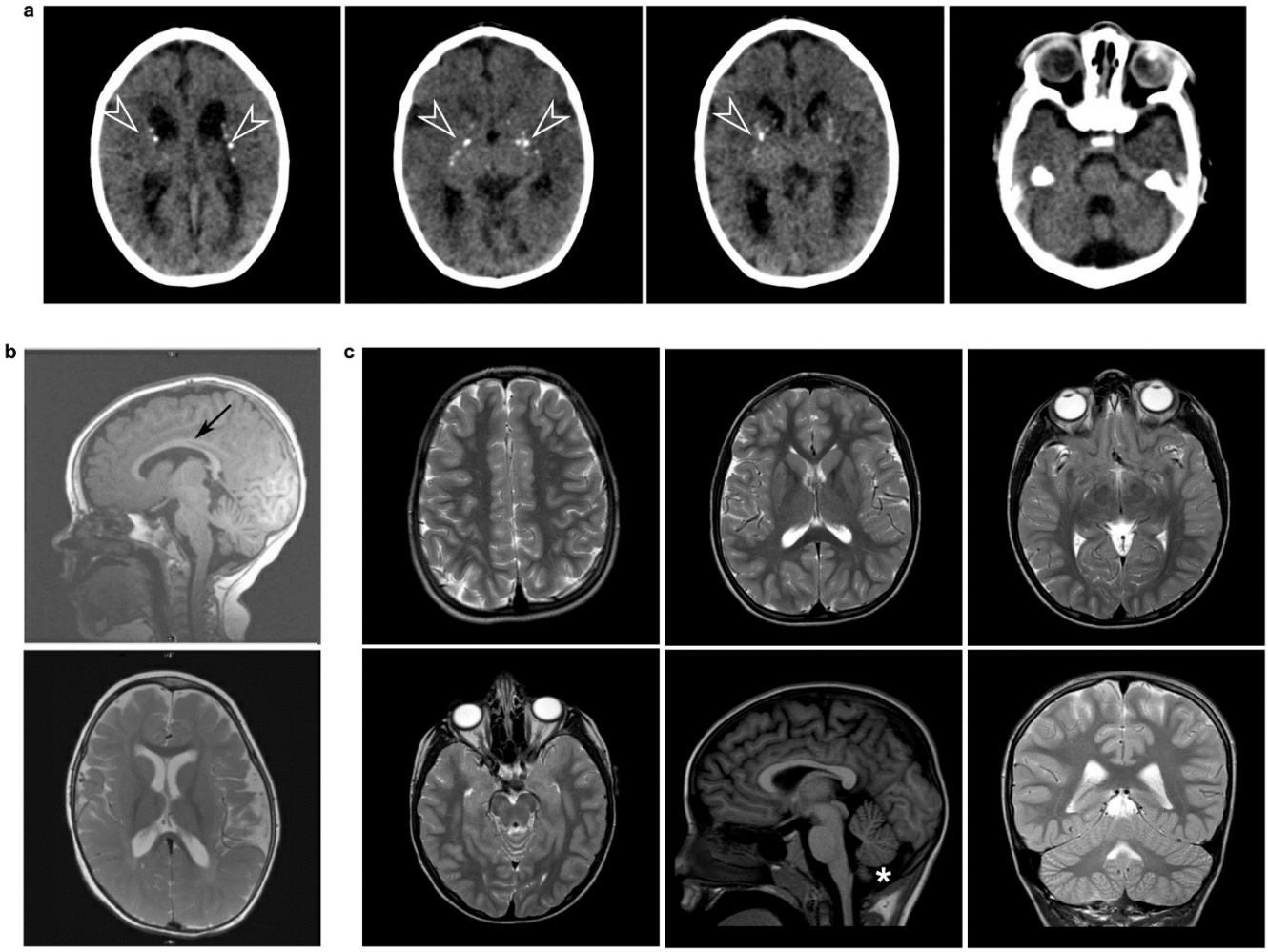

Extended Data Figure 4: Neuroimaging of other cases with DENND5A-related DEE show varying levels of phenotypic overlap. a, CT from a homozygous individual with the variant p.V1202Afs*52 (participant 25) shows mild cortical volume loss, ventriculomegaly, thin corpus callosum, and lenticulostriate and periventricular calcifications (arrowheads). **b,** MRI from a compound heterozygous individual with variants c.950-20_950-17delTTTT/p.R1078Q (participant 9) shows mild corpus callosum volume loss (arrow). **c,** MRI from a compound heterozygous individual with variants p.K485E/p.R1159W (participant 8) shows a normal MRI with mild inferior cerebellar vermis hypoplasia (asterisk).

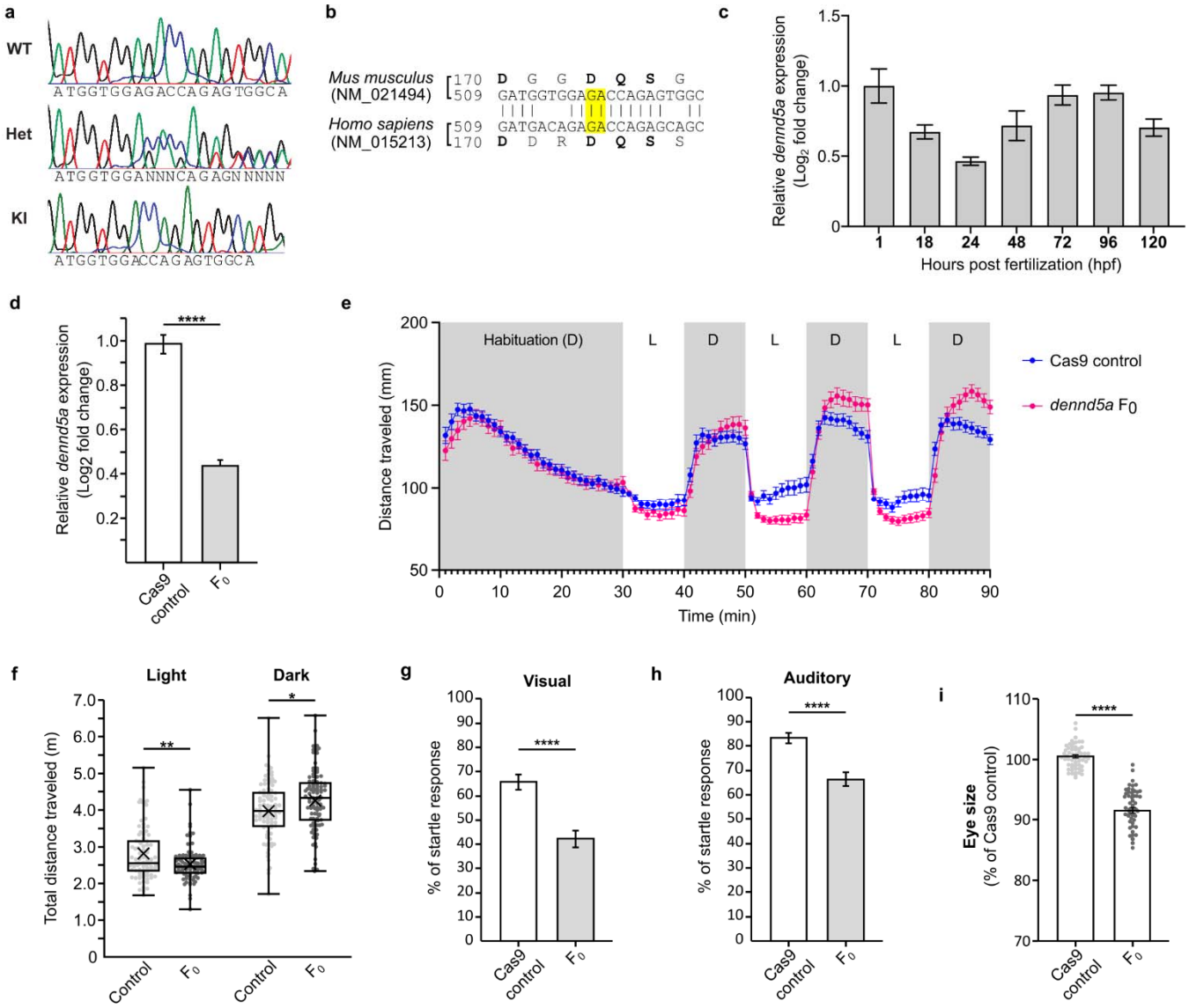

Extended Data Figure 5: Features of *DENND5A* transgenic animals make them valid models to study *DENND5A*-related DEE. a, Sample chromatograms demonstrating DENND5A DNA sequences in WT, heterozygous (Het), and knock-in (KI) mice. **b,** DNA and amino acid sequence alignment between human and mouse DENND5A sequences. Highlighted base pairs indicate bases deleted using CRISPR/Cas9. **c,** The temporal expression of zebrafish *dennd5a* mRNA by RT-qPCR at different developmental stages from experiments performed with biological and technical triplicates. Expression levels were normalized to the *18S* housekeeping gene and compared to 1 hpf embryos. Error bars = mean ± SD. **d,** Expression of *dennd5a* mRNA in Cas9 controls and *dennd5a* F_0 knockouts detected by RT-qPCR at 5 dpf. Experiments were performed with four biological replicates with technical triplicates. Data are mean ± SEM analyzed via two-tailed student's *t*-test ($t(6) = 10.706$, $p < .0001$). **e,** Locomotor activities of zebrafish larvae at 5 dpf with n = 96 larvae for each group. Data are mean ± SEM. D = Dark period, L = light period. **f,** Quantification of distance traveled by each larva during the

cycles of light or dark periods analyzed via two-tailed Mann-Whitney U test (light; $Z = -2.81$, $p = .005$) and two-tailed student's *t*-test (dark; $t(190) = -2.438$, $p = .016$). Each dot represents one larva. **g,** Visual startle response in $n = 143$ larvae at 6 dpf. Data are mean ± SEM analyzed via two-tailed Mann-Whitney U test ($Z = -4.957$, $p < .0001$). **h,** Acoustic evoked behavioral response in $n = 134$ larvae at 6 dpf. Data are mean ± SEM analyzed via two-tailed Mann-Whitney U test ($Z = -4.947$, $p < .0001$). **i,** Quantification of eye size in $n = 60$ larvae. Each dot represents one larva. Data are mean ± SEM analyzed via two-tailed Welch's *t*-test ($t(96.016) = 17.831$, $p < .0001$).

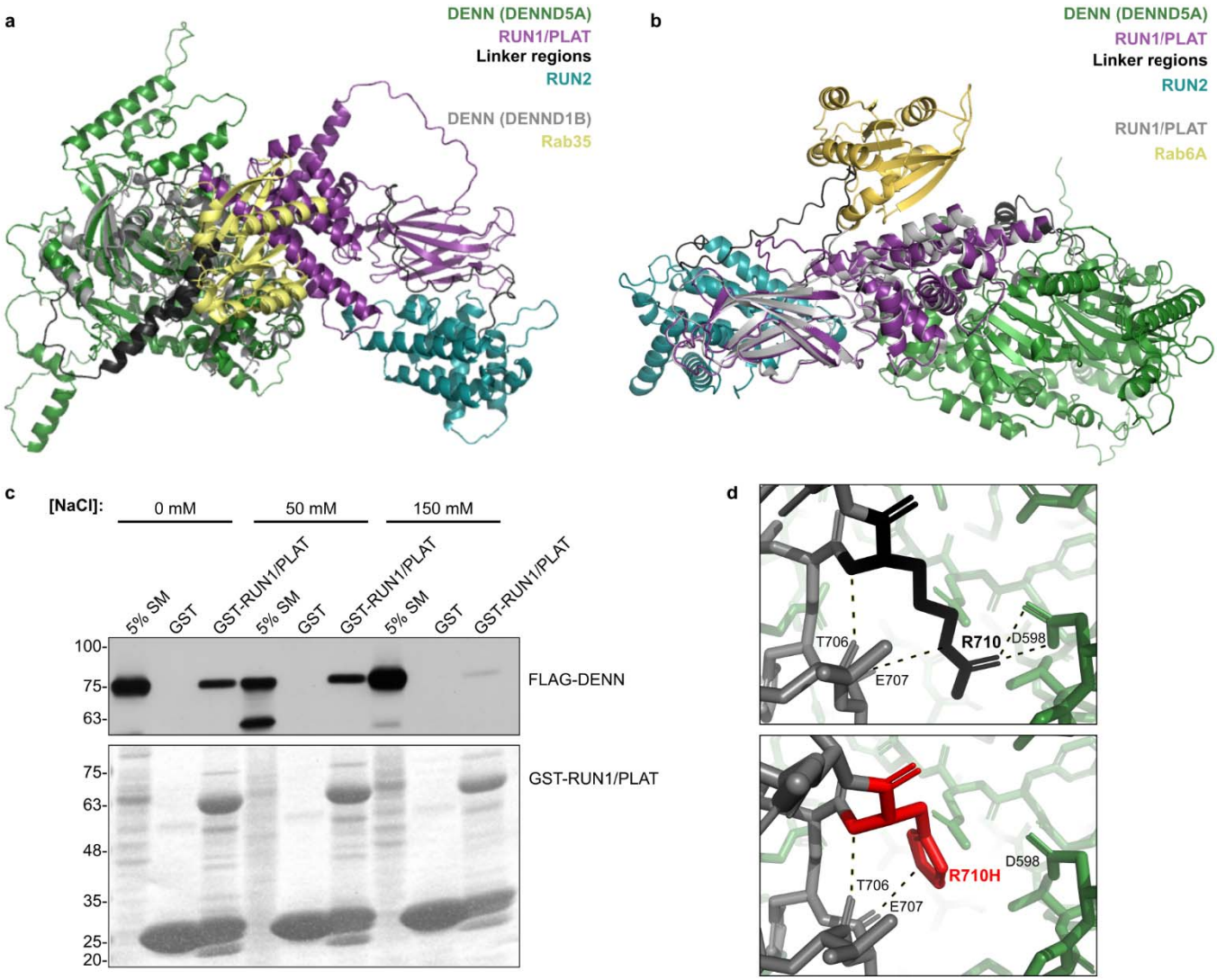

Extended Data Figure 6: Analysis of the predicted DENND5A structure indicates intramolecular interactions may regulate other protein-protein interactions. a, Structural alignment between the predicted DENND5A structure and PDB:3TW8 (gray, yellow) **b,** Structural alignment between the predicted DENND5A structure and PDB:3CWZ (gray, yellow) **c,** Pulldown experiment showing binding capacity between GST-RUN1/PLAT and FLAG-DENN domains of DENND5A under varying NaCl concentrations. **d,** The R710H variant found in the cohort and within the region that interacts with PALS1/MUPP1 results in the removal of two hydrogen bonds with D598 of the DENN domain. Dotted lines indicate hydrogen bonds.

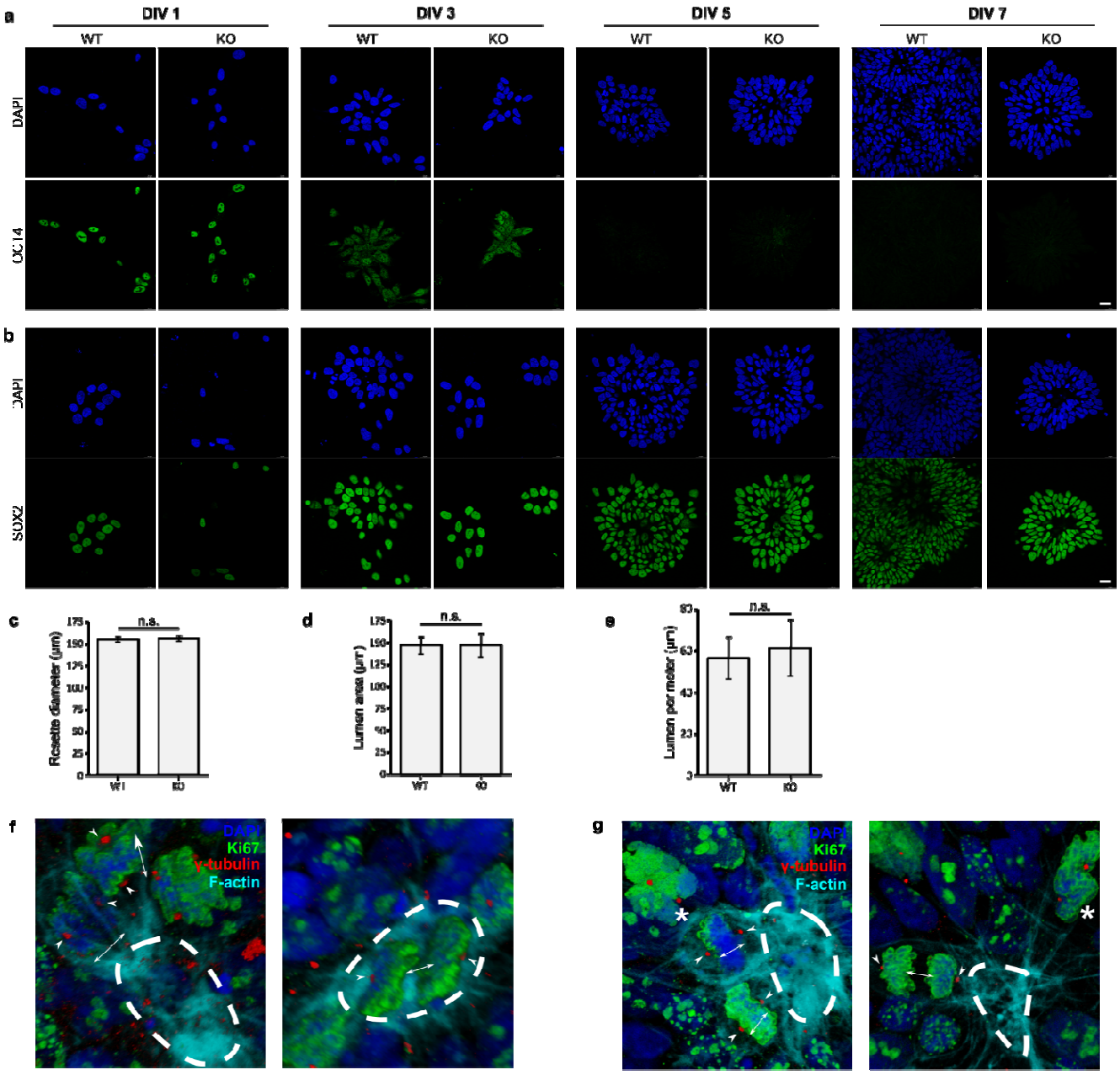

Extended Data Figure 7: WT and *DENND5A* KO neural rosettes differ in density and cell division properties, but not in marker expression or size. Expression of **a,** OCT4 and **b,** SOX2 during neural rosette development. Blue = DAPI, green = OCT4/SOX2. Scale bars = 20 µm. **c,** Average diameter of individual rosettes. *n* = 159 rosettes were analyzed from 2 independent experiments. Data are mean ± SEM and analyzed via student's *t*-test. **d,** Average lumen area of rosettes. *n* = 294 rosettes were analyzed from 2 independent experiments. Data are mean ± SEM and analyzed via Mann-Whitney U test. **e,** Average lumen perimeter of rosettes. *n* = 294 rosettes were analyzed from 2 independent experiments. Data are mean ± SEM and analyzed via Mann-Whitney U test. **f,** 3D-rendered images of apical progenitors of WT neural rosettes. Blue = DAPI, green = Ki67, red = -tubulin, cyan = F-actin. Arrowheads indicate centrosomes, arrows indicate orientation of cell divisions, dotted lines indicate the lumen. **g,** 3D-

rendered images of apical progenitors of KO neural rosettes. Blue = DAPI, green = Ki67, red = -tubulin, cyan = F-actin. Arrowheads indicate centrosomes, arrows indicate orientation of cell divisions, asterisks indicate abnormally condensed chromatin, dotted lines indicate the lumen.

Acknowledgements

We would like to acknowledge all cohort members in this study, their families, and treating clinicians for their participation. Participant 10 was recruited as part of the German-Jordanian Autosomal Recessive Intellectual Disability project (GeJo-ARID) funded by the German Academic Exchange Service (DAAD) as part of the German-Arab Transformation Program Line4 (Project-ID 57166498). The views expressed are those of the author(s) and do not reflect the official policy of the Department of the Army, the Department of Defense or the U.S. Government. The content is solely the responsibility of the authors and does not necessarily represent the official views of the National Institutes of Health. This work was funded by a Foundation Grant from the Canadian Institutes of Health Research to PSM, and a grant from the Alain and Sandra Bouchard Foundation for Intellectual Disabilities to PSM and TMD. This work was also supported by the King Salman Center for Disability Research through Research Group no RG-2022-010 (FSA). This work was also performed under the Care4Rare Canada Consortium funded by Genome Canada and the Ontario Genomics Institute (OGI-147), the Canadian Institutes of Health Research, Ontario Research Fund, Genome Alberta, Genome British Columbia, Genome Quebec, and Children's Hospital of Eastern Ontario Foundation (DC, ESYG, MO). Research reported in this manuscript was also supported by the NIH Common Fund, through the Office of Strategic Coordination/Office of the NIH Director under Award Number(s) [U01HG007672, U01HG007943] (HC) and [NS105078, HG011758] (JRL).

Author Contributions

EBan designed, performed, and analyzed most experiments and wrote the manuscript. VFr performed mouse immunohistochemistry, coordinated induced seizure experiments and mouse MRIs, and maintained the mouse colony. SJL performed and analyzed zebrafish experiments in Fig. 4 and Extended Data Fig. 5. FK established the mouse colony and performed the western blot in Fig. 3a. VFo processed and analyzed mouse MRIs. ML performed the induced seizure experiments. CH established the iPSC lines. GK performed RT-qPCR on mouse brain tissue for Fig. 3b. MT performed the mouse MRIs. AB analyzed mouse MRIs and provided experimental input. FSA generated and provided lymphoblast cell lines and contributed two clinical cases. SH and SK established iPSC lines from participants 2 and 10. RM identified many cohort members and provided pedigrees for Extended Data Fig. 1. RAK, FSA, LA, MBab, MBah, BB, EBar, LB,

MBas, MBer, DB, RB, Mbu, MC-D, DCa, HC, DCu, SE, MAE, HGES, TF, HKG, JGG, LG, ESYG, VKG, TBH, MOH, TLH, JSH, AH, HH, KH, SH, EGK, GCK, AK, HL, JRL, EJM, AM, DM, JN-F, HN, DN, BO-J, MO, DP, LGS, CS, LS, VS, RCS, VMS, MSZ, DZ, and CZ completed phenotypic questionnaires and contributed to clinical phenotyping genetic analysis. KM acted as a liaison to connect EBan with clinicans that submitted variants on ClinVar. RP analyzed clinical exomes of GeneDx-tested cases. BAM identified the initial cases. UDN is associated with the contribution of data from participant 9. KH and CP provided technical aid to F_0 zebrafish experiments. J-FT identified the intramolecular interface in Fig. 4 and supervised all structural analyses. TMD supervised iPSC quality control and cell line production. ZG supervised genetic analysis. MA supervised induced seizure experiments. CA analyzed participant MRIs and CTs. GKV supervised zebrafish experiments. RM contributed many clinical cases and connected us with CA, GKV, SJL, KH, and CP. All authors reviewed the manuscript for accuracy and edited wording or data presentation according to their clinical, molecular, structural, genetic, or biological expertise. PSM supervised the study, designed experiments, secured funding, and wrote the manuscript.

Competing Interests

KM and RP are employed by GeneDx, LLC. All other authors report no conflicts of interest.

Additional Information

Supplementary Information is available for this paper.

Correspondence and requests for materials should be addressed to PSM.

Reprints and permissions information is available at www.nature.com/reprints.

Methods

Participant Recruitment

All materials and methods for participant recruitment and clinical data collection was approved by the McGill University Health Centre research ethics board (study 2021-6324) and the McGill Faculty of Medicine and Health Sciences institutional review board (study A12-M66-21B). We originally identified four individuals, one deceased and excluded from the cohort, from two consanguineous families with homozygous *DENND5A* variants[1]. Another two homozygous individuals were briefly described by Anazi *et al*. in 2017 and were recruited into the study[2]. We identified an additional 23 individuals with *DENND5A* variants: 15 were brought to our attention by clinicians who reached out to us after performing diagnostic whole exome sequencing on patients; 5 were identified through physician-submitted GeneMatcher[3] and ClinVar[4] database entries; and 3 were identified through word-of-mouth of the study between clinicians that already completed the survey and their colleagues with other *DENND5A* cases. Recruitment spanned approximately four years. Six individuals were excluded from the cohort and subsequent analysis: two did not meet eligibility criteria (both are heterozygous for a *DENND5A* variant, having only one affected allele); one was excluded due to death occurring prior to clinical data collection[1]; and three were excluded because the questionnaires were not returned.

Phenotypic data collection and analysis

Clinicians with patients harboring *DENND5A* variants of unknown or likely pathogenicity completed an anonymized phenotypic questionnaire based on their patient's most recent clinic visit. Available anonymized MRIs, CTs, and/or or official reports were contributed if the patient underwent neuroimaging for clinical purposes. Participants were assigned a numerical ID in the order in which their questionnaires were received. For intronic variant analysis, molecular consequences were predicted using Ensembl's Variant Effect Predictor. [5] For those whose raw MRI or CT data were provided, an independent neuroradiologist re-analyzed the scans and completed the "Brain" section of the questionnaire without viewing the original submitted questionnaires. If responses to an item differed between the original clinician and the independent radiologist, the independent radiologist's response was used for analysis. Data are missing if the presence of a phenotype is officially unknown. For occipitofrontal circumference

(OFC), if percentiles were not given directly from clinicians, percentile values were derived from the age- and sex-appropriate Word Health Organization tables (https://www.who.int/tools/child-growth-standards/standards/head-circumference-for-age). The OFC percentile for one person whose measurements were taken when they were above 5 years old was derived from tables published in Adela Chirita-Emandi et al[6]. For calculating central tendency statistics, OFC percentiles given as a range (e.g. < 3 or < 1) were assigned a conservative numerical estimate (e.g. 2.9 for < 3, 0.9 for < 1).

Establishment of cell lines

The control induced pluripotent stem cell (iPSC) line AIW001-02 was derived from peripheral blood mononuclear cells of a healthy female donor (Caucasian, 48 years old). The AIW001-02 cell line was generated by using the CytoTune™-iPS 2.0 Sendai Reprogramming Kit (iPSQuebec Platform, Laval University). For knockout expression of human *DENND5A*, guide RNAs (gRNAs) were designed using an online tool (https://benchling.com). Both gRNA target sites are on *DENND5A* exon 4. Synthesized gRNAs were ordered from SYNTHEGO and transfection was performed following the manufacturer's protocol. Single cell colonies were picked and amplified. Genomic DNA from the colonies was extracted with QuickExtract (Lucigen) and PCR was performed using Q5 High-Fidelity DNA Polymerase according to the manufacturer's protocol (F: GAGGATCGCCAGTGAGTGTT; R: CCCCGAGCAGTTCAAAAACC). A 238 base pair deletion was confirmed by Sanger sequencing.

Human fibroblasts from DENND5A cohort members were obtained by skin biopsy (participant IDs: 2 and 10) and renal epithelial cells (participant ID: 3) from a urine sample. Cells were reprogrammed to iPSCs by electroporation with episomal plasmids (pCXLE-hUL, pCXLE-hSK, and pCXLE-hOCT4) as previously described[7]. Generated iPSCs were functionally and genomically validated according to Hauser and Erzler[8].

Lymphoblasts were obtained from a healthy individual (control line) and two homozygous patients (participant IDs: 4 and 5). Cells were immortalized through use of the Epstein-Barr virus and generated in the lab of Dr. Fowzan Alkuraya.

Cell culture

iPSCs were cultured on hESC-qualified Corning Matrigel-coated tissue culture dishes in either TeSR-E8 medium (all patient-derived iPSC lines; STEMCELL Technologies) or mTeSR1 medium (AIW001-02 WT and *DENND5A* KO; STEMCELL Technologies) with daily medium changes and mechanical removal of differentiated cells. Cells were passaged using the ReLeSR Passaging Reagent (STEMCELL Technologies) once cultures reached approximately 70% confluency.

iPSCs were differentiated to neural progenitor cells (NPCs) using the STEMdiff SMADi Neural Induction Kit (STEMCELL Technologies) with daily medium changes. Induced cultures were passaged using Accumax (Millipore Sigma) once cells reached 90-95% confluency, approximately once per week. After a two week induction period, NPCs were maintained in STEMdiff Neural Progenitor Medium (STEMCELL Technologies) on poly L ornithine (PLO)- and laminin-coated plates and passaged using Accumax once cultures reached 80-95% confluency, approximately once per week. Experiments examining β-III tubulin expression examined established NPC lines after one passage post-neural induction; all other experiments were performed using cells at passages 2-4.

Control and patient-derived Epstein-Barr virus-induced lymphoblastoid cell lines were obtained from the laboratory of Dr. Alkuraya. Cells were cultured in suspension in RPMI 1640 medium (Gibco) supplemented with 15% fetal bovine serum (Wisent), 1% penicillin-streptomycin (Wisent), and 1% L-glutamine (Wisent). Cells were split 1:4 once confluency reached approximately 1 x 10^6 cells/ml.

For biochemical studies, HEK293-T cells were cultured in DMEM high glucose (Fisher) supplemented with 10% bovine calf serum (Fisher), 1% L-glutamine (Wisent), and 1% penicillin-streptomycin (Wisent).

Plasmid cloning

DENND5A cDNA (Origene, SC121400) was cloned into the pCMV-tag2B vector to generate FLAG-DENND5A. GFP-DENND5A was made via subcloning DENND5A into the pEGFP-C1 vector. Patient variants and targeted residues for biochemical studies were introduced using the QuikChange Lightning site-directed mutagenesis kit (Agilent) following the manufacturer's protocol. FLAG-DENND5A DENN domain was made by subcloning aa1-680 of DENND5A

into the pCMV-tag2B vector. GST-aa700-720 was made via oligo annealing followed by ligation into a pGEX-4T1 vector with a modified multiple cloning site (MCS). GST-RUN1/PLAT was created by subcloning DENND5A aa707-1090 into the pGEX-6P1 vector. MUPP1 (MPDZ) was obtained from the Harvard Medical School plasmid collection (HsCD00352820). His-Lin-7C was obtained from the lab of Dr. Andrew Rice from Baylor College of Medicine. Untagged PALS1 (MPP5) in pDONR223 was obtained from Addgene (#23447) and subcloned into a pCMV3-C-FLAG vector to generate PALS1-FLAG. The vector backbone from PALS1-FLAG was then isolated and modified to include a custom MCS via oligo annealing and ligation in order to create restriction sites suitable for subcloning MUPP1 into the vector. MUPP1 was subcloned into this modified vector to create MUPP1-FLAG. All constructs were confirmed by Sanger sequencing.

RT-qPCR

RNA was extracted from NPCs and lymphocytes using the RNeasy kit (Qiagen) followed by cDNA synthesis using iScript Reverse Transcription Supermix for RT-qPCR (Bio-Rad). RT-qPCR was performed using SsoFast EvaGreen Supermix (Bio-Rad) with primers targeting human *DENND5A* (F: CTAAAGCCAGGGATGGTGCC; R: TTTCGGCATACATAGCATTCCT) and *TBP* (F: TGCACAGGAGCCAAGAGTGAA; R: CACATCACAGCTCCCCACCA). *DENND5A* levels were normalized to *TBP* levels and AIW001-02 WT NPCs or control lymphocytes.

RNA from mouse brain tissue was extracted using RNeasy Lipid Tissue kit (Qiagen), followed by cDNA synthesis and RT-qPCR performed with the same reagents as above using primers specific to the mouse genome for *DENND5A* (F: CAGTCGCTTCGCCGACTAT; R: GCACCATCCCTGGCTTTAGAA) and *GAPDH* (F: ACTCCACTCACGGCAAATTC; R: CCAGTAGACTCCACGACATACT). *DENND5A* levels were normalized to *GAPDH* levels in WT mice.

RNA was extracted from zebrafish samples using TRIzol Reagent (Thermo Fisher Scientific) and purified with the RNA Clean and Concentrator-5 kit (Zymo Research) according to the manufacturer's guidelines. cDNA was synthesized using iScript Reverse Transcription Supermix (Bio-Rad). RT-qPCR was performed on the Light Cycler 96 System (Roche) using specific primers for zebrafish *dennd5a* (F: TTGGCGAGTGCAAATGAAGG; R:

GTTTGCTGGTCACCTCCTCA) along with SYBR Green Supermix (Thermo Fisher Scientific). *dennd5a* expression levels were normalized to the *18S* gene and the 1 hpf stage (in temporal *dennd5a* expression analysis) or to Cas9-injected control animals (to analyze *dennd5a* expression in control versus F_0 KO animals).

Neural rosette formation assay

iPSCs were gently dissociated into a single cell suspension and plated at low density (20,000 cells per well of a 24 well plate) onto PLO/Laminin-coated coverslips in neural induction media with SMAD inhibitor (STEMCELL Technologies #08581) containing 10 µM Y-27632 on the day of plating. Medium was changed daily and cells were fixed after 1, 3, 5, and 7 days in culture. Rosettes were stained and z-stack images in 0.5 µm increments were taken using the Leica SP8 confocal microscope. For lumen size analysis, z-plane images with the largest visible lumens were used for quantification followed by two-tailed student's *t*-tests. For rosette diameter analysis, z-plane images with the widest phalloidin staining were used for quantification followed by a two-tailed student's *t*-test. To analyze dividing cells within the rosettes, cells in metaphase, anaphase, and telophase were used for quantification. Mitotic spindle angles were measured as in Chilov et al., 2011[9] using ImageJ.

Immunocytochemistry

Samples were fixed in 4% paraformaldehyde for 20 minutes at room temperature. Cells were permeabilized for 5 minutes in 0.1% Triton-X 100 and then blocked in 5% BSA and 0.01% Triton-X 100 in PBS for 30 minutes at room temperature, followed by overnight incubation at 4°C with the following antibodies: OCT4 (ab19857, 1 µg/ml), SOX1 (Invitrogen MA1-109, 1:200), SOX2 (Abcam ab92494, 1:1000), Nestin (Invitrogen, MA1-110), β-III tubulin (Abcam ab52623, 0.1 µg/ml), Ki67 (Abcam ab15580, 0.5 µg/ml), γ-tubulin (Sigma-Aldrich T6557, 1:500), and Pals1 (Santa Cruz Biotechnology sc-365411, 1:350). After primary antibody incubation, samples were washed twice with PBS then incubated with Alexa-conjugated secondary antibodies at 1:500 dilution and phalloidin at 1:1000 dilution for 1 hour at room temperature. Cells were then washed twice in PBS, incubated with DAPI at 1:5000 dilution for 10 minutes, washed twice in PBS again, and mounted onto glass slides.

Endogenous and transfected protein expression

NPCs and lymphoblasts were harvested in lysis buffer (20 mM HEPES pH 7.4, 100 mM NaCl, 0.83 mM benzamidine, 0.5 µg/ml aprotinin, 0.5 g/ml leupeptin, 0.23 mM phenylmethylsulfonyl fluoride) containing 1X LSB. Mouse brains were homogenized in lysis buffer and incubated with 1% Triton X-100 for 15 minutes at 4°C, followed by centrifugation at 239,000 x *g* for 15 minutes at 4°C. For FLAG-DENND5A expression, plasmid DNA was transfected into HEK293T cells using the calcium phosphate method and cells were harvested after 24 hours in lysis buffer containing 1X LSB. Equal protein aliquots were loaded onto an SDS-PAGE gel and analyzed via Western blot using primary antibodies against DENND5A (ThermoFisher #702789, 2.5 µg/ml), FLAG (clone M2, Sigma-Aldrich, 1:10,000), Hsc70 (clone 1B5, StressGen Biotechnologies Corp, 1:1:10,000), and β-actin (Clone C4, Sigma-Aldrich MAB1501R, 1:1000).

Pulldown experiments

500 mL flasks of bacteria were induced overnight at RT to express GST-tagged proteins using 500 µM IPTG when the optical density of the cultures at 600 nm reached 0.6. Bacteria were pelleted and resuspended in PBS + protease inhibitors pH 7.4. Resuspended bacterial cells were then sonicated 3 times for 5 seconds at 70% amplitude, followed by incubation with 1% Triton X-100 for 15 minutes. Bacterial cell lysate was then spun for 5 minutes at 4°C at 11,952 x *g*. The supernatant was incubated with glutathione Sepharose beads pre-washed 3 times in PBS for one hour at 4°C, and beads were then briefly spun down and washed 3 times in PBS + protease inhibitors to purify GST fusion proteins. The concentration of fusion proteins was determined by running on an SDS-PAGE gel accompanied by a BSA standard curve followed by Coomassie Brilliant Blue staining. Cell lysates were then harvested for incubation with GST fusion proteins. For the initial protein-protein interaction screen followed by mass spectrometry, E18 rat brains were homogenized on ice in lysis buffer (20 mM HEPES pH 7.4, 150 mM NaCl, 0.83 mM benzamidine, 0.5 µg/ml aprotinin, 0.5 µg/ml leupeptin, and 0.23 mM phenylmethylsulfonyl fluoride) with 10 strokes using a Caframo homogenizer at 1200 rpm. Tissue homogenate was then sonicated once for 10 seconds at 20% amplitude, incubated in 1% Triton X-100 for 15 minutes at 4°C, and spun at 239,000 x *g* and 4°C for 15 minutes. For pulldown experiments with overexpressed proteins, HEK293-T cells were transfected using the calcium phosphate method with the appropriate plasmids and harvested the next day in lysis buffer. Cells were then sonicated once for 10 seconds at 20% amplitude, incubated in 1% Triton X-100 for 15 minutes at

4°C, and spun at 21 x *g* and 4°C for 15 minutes in a tabletop centrifuge. The concentration of the rat brain and HEK293T supernatants were analyzed via a Bradford assay, and 1 mg/ml was incubated with 25 µg (GST-aa700-720) or 50 µg (GST-RUN1/PLAT) of fusion proteins for one hour at 4°C. Following incubation, beads were washed 3 times in buffer containing 1% Triton, eluted in 1X Lammeli sample buffer (LSB), loaded onto an SDS-PAGE gel, and analyzed via Western blot using primary antibodies against FLAG (clone M2, Sigma-Aldrich, 1:10,000).

Co-immunoprecipitation experiments

For co-immunoprecipitation experiments, HEK293-T cells were transfected using the calcium phosphate method, harvested in lysis buffer, and sonicated once for 10 seconds at 20% amplitude, followed by incubation in 0.5% Triton X-100 for 15 minutes at 4°C. Cell lysate was then spun at 21 x *g* and 4°C for 15 minutes in a tabletop centrifuge, and 1 mg/ml of the resulting supernatant was incubated for one hour at 4°C with 25 µl ChromoTek GFP-Trap Agarose magnetic beads pre-equilibrated 3 times in lysis buffer without Triton X-100. Beads were then washed 3 times in lysis buffer containing 0.05% Triton and then eluted in 1X LSB for SDS-PAGE analysis and analyzed via Western blot using primary antibodies against FLAG (clone M2, Sigma-Aldrich, 1:10,000) and GFP (Invitrogen Cat# A-6455, 1:20,000).

Animal care and selection

All mouse care and experiments in the study were approved by the Montreal Neurological Institute Animal Care Committee in accordance with guidelines set by the Canadian Council on Animal Care under ethical protocol number 5734. The experimental unit for this study is a single animal. Apart from selecting animals based on *DENND5A* genotype, no exclusion criteria were set for the experiments and both male and female animals were used.

Crispant zebrafish experiments used wild-type strain NHGRI-1[10] according to the protocol approved by the Institutional Animal Care Committee (IACUC) of Oklahoma Medical Research Foundation (22-18). All animals were raised and maintained in an Association for Assessment and Accreditation of Laboratory Animal Care (AAALAC) accredited facility under standard conditions.

Establishment of transgenic animal models

KI mice were generated by the McGill Integrated Core for Animal Modeling. Two silent mutations were introduced in L168 and L169 (CTTGCT –> TTAGCA) as well as a deletion of 2 bp in G172 to introduce a frameshift and premature stop codon in exon 4 of the *DENND5A* mouse gene. Briefly, custom sgRNAs (Synthego), Cas9 protein (IDT, Cat#1081058) and ssODN (ultramer, IDT) were microinjected into the pronucleus of C57BL/6N mouse zygotes with concentrations of 50:50:30 ng/µl respectively. Embryos were subsequently implanted in CD-1 pseudopregnant surrogate mothers according to standard procedures approved by the McGill University Animal Care Committee. Founder pups (F0) were genotyped for evidence of a deletion of 2 bp in G172 and mated to wild-type C57BL/6N (Charles River) mice for three generations. The colony was maintained by sibling mating and by crosses to C57BL/6N mice every third generation. All genomic sequencing was performed using the Big Dye Terminator Ready Reaction Mix (ABI, Carlsbad, CA, USA) at the McGill and Genome Quebec Innovation Center (Primers: ACAAGGAATGCTCTCACTGC, CACACTCCGACATGCCTTCAT [417 bp]). Obtained sequences were analyzed using an online tool (https://benchling.com).

Previously described methods were used to generate *dennd5a* KO zebrafish in crispant experiments[11,12] using single-guide RNAs (sgRNAs) designed using the CRISPOR tool targeting three *dennd5a* sites (GGTGTTTGAGCTGCTAGGGC, GGGCTGATCTGACAGGAAGG, AGATGGGCCATGATAACTCA) and synthesized by in vitro transcription. Embryos at the one-cell stage were injected with a mixture containing Cas9 protein with (F_0 knockouts) or without (control) sgRNAs.

4-aminopyridine induced seizure assay

Mice were injected with the K+ channel blocker 4-aminopyridine (8 mg/kg, i.p.) (Sigma-Aldrich, Canada) to induce seizures. If no seizures were observed after 30 min, they were re-injected with a half-dose of 4-aminopyrdine (4 mg/kg, i.p.). Animals that showed no seizures after the second dose were excluded from further analysis. Seizures were identified based on behavioral symptoms such as myoclonic activity of rear and forelimbs that evolved to rearing and loss of balance. The latency (min) from the time of the last 4-aminopyridine injection and seizure onset was calculated.

Zebrafish morphological and behavioral phenotyping

Morphological phenotyping was conducted by randomly selecting Cas9-injected control and F_0 KO animals at 5 days post fertilization (dpf) and anesthetizing them with Tricaine/MS-222 (Sigma-Aldrich). The animals were positioned in 2% methylcellulose (Sigma Aldrich) under a stereomicroscope and imaged using a high-definition Nikon DS-Fi2 camera mounted on a Nikon SMZ18 stereomicroscope. Head and eye sizes were measured from scale-calibrated images using ImageJ.

All behavioral tests were conducted at room temperature. Acoustically evoked behavioral response tests were carried out using Zebrabox behavior chambers (Viewpoint Life Sciences) as previously described[12] involving the percentage of responses for 12 stimuli per larva. The visual startle response test was performed using the DanioVision system running EthoVision XT software (Noldus Information Technology, Leesburg), as previously reported[12,13] based on the number of responses for five stimuli per larva. For locomotor behavior recording during light/dark transitions, 4 dpf larvae were transferred to a 96-well plate, with one larva per well in 150 µL of embryo water. The following day, the plate was placed in a Noldus chamber, and the DanioVision system running EthoVision XT software was used to record locomotion activity. The 5 dpf larvae underwent a 30-minute habituation period in the light, followed by three cycles of 10-minute light and 10-minute dark transitions. The locomotion activity of the larvae was recorded as the distance traveled in millimeters (mm) per minute.

Whole-mount in situ hybridization (WISH)

WISH was performed on zebrafish embryos using a previously described method[14] using a 673-bp amplicon of zebrafish dennd5a cDNA produced via PCR (Primers: T3-dennd5a_F: gaattgaattaaccctcactaaagggCGAGTGCAAATGAAGGTGAG; T7-dennd5a_R: gaattgtaatacgactcactatagggGGTCTCTGACAGATCACTGG).

Immunohistochemistry

Mouse brain sections were baked overnight at 60°C in a conventional oven. Samples were then deparaffinized and rehydrated in a series of xylene and ethanol washes, followed by antigen retrieval using citrate buffer (pH 6.0) for 10 minutes at 120°C in a decloaking chamber (Biocare Medical). Slides were then rinsed IHC buffer (PBS + 0.05% Tween-20 + 0.2% Triton X-100) and blocked for 1 hour with Protein Block (Spring Bioscience), incubated with primary

antibodies overnight at 4°C, and washed with IHC buffer followed by incubation with respective secondary antibodies (Invitrogen) for 1 hour at room temperature. Coverslip mounting was done using ProLong Diamond Gold Antifade Mountant with DAPI (Invitrogen) to stain nuclei. mages were acquired using Leica SP8 laser scanning confocal microscope. Quantification of the percentage of cells per mm^2 labeled by NeuN or GFAP was based on three 10x magnification images per animal from a total of $n = 4$ mice. Cells within 100 µm of the ependymal layer (excluding the ependymal cells) in which DAPI signal was also evident were considered. All measurements were done using ImageJ.

For zebrafish, 6 dpf larvae were first blocked in blocking buffer (10 % Goat Serum, 1% BSA, 1% DMSO and 0.5 % Triton X-100 in PBS) overnight at 4°C, followed by incubation with primary antibodies, including mouse IgG2b anti-acetylated tubulin (1:200; Sigma-Aldrich) and anti-SV2 (1:200; DSHB), for 5 days with gentle agitation in a cold room. After washing 3 times with PBSTx, larvae were incubated with secondary antibodies, including goat anti-rabbit IgG Alexa Fluor 488 (1:500, Jackson ImmunoResearch) and goat anti-mouse IgG Alexa Fluor 647 antibody (1:500, Jackson ImmunoResearch, PA) for 3 days at 4°C. Following a series of washes, larvae were laterally mounted in 1.5% low melting point agarose (Sigma-Aldrich), and images were obtained using the Zeiss LSM-710 Confocal microscope.

7 T small animal MRI

Ten WT (3 males, 7 females, mean age = 114 days, *SD* = 12.9) and 10 KI (3 males, 7 females, mean age = 108 days, *SD* = 10.3) for a total of 20 mice were employed for high resolution, pre-clinical MR imaging experiments. Data from four animals were excluded from analysis to restrict subjects to an age range of approximately 3-4 months for consistency. For *in vivo* structural MRI, mice were anesthetized with isoflurane, placed in a plastic bed and restrained with gauze pads to minimize the possible influence of motion artifacts. For the duration of each MRI scan, mice were maintained under isoflurane gas anesthesia at approximately 37°C using a warm air blower and respiration was monitored using a pressure pad.

Imaging was performed using the 7 T Bruker Pharmascan (Bruker Biosciences, Billerica, MA), ultra-high field, pre-clinical MRI system of the McConnell Brain Imaging Centre at McGill University. The Pharmascan is equipped with an AVANCE II-model spectrometer and BFG-

150/90-S shielded gradient system (Resonance Research Inc., Billerica, Massachusetts). Structural MR images were acquired using a 2D Rapid Imaging with Refocused Echoes (RARE) pulse sequence with the following parameters: effective echo time (TE_{eff}): 30 ms, RARE factor: 8. In-plane resolution: 100 µm x 100 µm, slice thickness: 300 µm and receiver bandwidth: 46875 Hz. The repetition time (TR) and the number of acquired slices were varied for two pairs of WT/KO mice in order to achieve greater slice coverage along the rostro-caudal axis (TR: 4000 ms to 4750 ms, number of slices: 40 to 50). The number of averages was varied to optimize total scan time for mouse imaging under gas anesthesia. Mice were euthanized at the end of the experiment. Lateral ventricles were manually segmented in each scan by a researcher blind to animal genotypes using the ITK-SNAP software (www.itksnap.org).[15] and pooled lateral ventricle volumes were used for statistical analysis.

Identification of regions of interest with reduced local volume

An image registration-based method was used to identify brain regions at the voxel level with significant local volume difference between WT and KI mice, as described in Zha *et al*.[16] Voxel-level statistical analyses were performed using RMINC version 1.5.3.0 software and statistical results were corrected for multiple comparisons using the false discovery rate method with a threshold of 10%. Brain regions in the KI mice showing evidence of reduced volume were referenced to the Allen mouse brain atlas to identify more specific neuroanatomical areas and nuclei in mice that displayed reduced volume.

Statistical Analysis

Continuous data were analyzed for normality and homogeneity of variance using Shapiro-Wilk tests ($n < 50$) or Kolmogorov-Smirnov ($n \geq 50$) tests and Levene tests. Student's *t*-tests were conducted when all assumptions were met. Welch's t-tests were conducted when homogeneity of variance assumptions were not met. The nonparametric equivalent (Mann-Whitney U test) was conducted when both normality of data and homogeneity of variance assumptions were not met. A p value of < 0.05 was considered statistically significant. Data were analyzed using SPSS, R version 4.1.2 with Companion to Applied Regression package version 3.0, and Tidyverse version 1.3.1 software. All statistical analyses included multiple replicates from several independent experiments.

Data availability

Supplementary table 1 includes all raw data obtained in the cohort study and describes a clinical description of each participant, as well as sums and averages of phenotypes for the whole cohort. Raw data concerning *in vitro* cell experiments and *in vivo* and *ex vivo* mouse experiments were generated at the Montreal Neurological Institute of McGill University. Source data for all major experiments in the study have been uploaded to Figshare and are additionally available in Supplementary Information.

Method References

1. Han C, Alkhater R, Froukh T, Minassian AG, Galati M, et al. Epileptic Encephalopathy Caused by Mutations in the Guanine Nucleotide Exchange Factor DENND5A. *Am J Hum Genet*. Dec 1 2016;**99**(6):1359-1367. doi:10.1016/j.ajhg.2016.10.006
2. Anazi S, Maddirevula S, Faqeih E, Alsedairy H, Alzahrani F, et al. Clinical genomics expands the morbid genome of intellectual disability and offers a high diagnostic yield. *Mol Psychiatry*. Apr 2017;**22**(4):615-624. doi:10.1038/mp.2016.113
3. Sobreira N, Schiettecatte F, Valle D, Hamosh A. GeneMatcher: a matching tool for connecting investigators with an interest in the same gene. *Hum Mutat*. Oct 2015;**36**(10):928-30. doi:10.1002/humu.22844
4. Landrum MJ, Lee JM, Benson M, Brown GR, Chao C, et al. ClinVar: improving access to variant interpretations and supporting evidence. *Nucleic Acids Res*. Jan 4 2018;**46**(D1):D1062-D1067. doi:10.1093/nar/gkx1153
5. McLaren W, Pritchard B, Rios D, Chen Y, Flicek P, et al. Deriving the consequences of genomic variants with the Ensembl API and SNP Effect Predictor. *Bioinformatics*. Aug 15 2010;**26**(16):2069-70. doi:10.1093/bioinformatics/btq330
6. Chirita-Emandi A, Doros G, Simina IJ, Gafencu M, Puiu M. Head Circumference References for School Age Children in Western Romania. *Rev Med Chir Soc Med Nat Iasi*. Oct-Dec 2015;**119**(4):1083-91.
7. Okita K, Matsumura Y, Sato Y, Okada A, Morizane A, et al. A more efficient method to generate integration-free human iPS cells. *Nat Methods*. May 2011;**8**(5):409-12. doi:10.1038/nmeth.1591

8. Hauser S, Erzler M, Theurer Y, Schuster S, Schule R, et al. Establishment of SPAST mutant induced pluripotent stem cells (iPSCs) from a hereditary spastic paraplegia (HSP) patient. *Stem Cell Res*. Nov 2016;**17**(3):485-488. doi:10.1016/j.scr.2016.09.022

9. Chilov D, Sinjushina N, Rita H, Taketo MM, Makela TP, et al. Phosphorylated beta-catenin localizes to centrosomes of neuronal progenitors and is required for cell polarity and neurogenesis in developing midbrain. *Dev Biol*. Sep 1 2011;**357**(1):259-68. doi:10.1016/j.ydbio.2011.06.029

10. LaFave MC, Varshney GK, Vemulapalli M, Mullikin JC, Burgess SM. A defined zebrafish line for high-throughput genetics and genomics: NHGRI-1. *Genetics*. Sep 2014;**198**(1):167-70. doi:10.1534/genetics.114.166769

11. Varshney GK, Carrington B, Pei W, Bishop K, Chen Z, et al. A high-throughput functional genomics workflow based on CRISPR/Cas9-mediated targeted mutagenesis in zebrafish. *Nat Protoc*. Dec 2016;**11**(12):2357-2375. doi:10.1038/nprot.2016.141

12. Lin SJ, Vona B, Barbalho PG, Kaiyrzhanov R, Maroofian R, et al. Biallelic variants in KARS1 are associated with neurodevelopmental disorders and hearing loss recapitulated by the knockout zebrafish. *Genet Med*. Oct 2021;**23**(10):1933-1943. doi:10.1038/s41436-021-01239-1

13. Lin SJ, Vona B, Porter HM, Izadi M, Huang K, et al. Biallelic variants in WARS1 cause a highly variable neurodevelopmental syndrome and implicate a critical exon for normal auditory function. *Hum Mutat*. Oct 2022;**43**(10):1472-1489. doi:10.1002/humu.24435

14. Thisse B, Thisse C. In situ hybridization on whole-mount zebrafish embryos and young larvae. *Methods Mol Biol*. 2014;**1211**:53-67. doi:10.1007/978-1-4939-1459-3_5

15. Yushkevich PA, Piven J, Hazlett HC, Smith RG, Ho S, et al. User-guided 3D active contour segmentation of anatomical structures: significantly improved efficiency and reliability. *Neuroimage*. Jul 1 2006;**31**(3):1116-28. doi:10.1016/j.neuroimage.2006.01.015

16. Zha C, Farah CA, Fonov V, Rudko DA, Sossin WS. MRI of Capn15 Knockout Mice and Analysis of Capn 15 Distribution Reveal Possible Roles in Brain Development and Plasticity. *Neuroscience*. Jun 15 2021;**465**:128-141. doi:10.1016/j.neuroscience.2021.04.023